January 2016

Copper Indium Sulfide Quantum Dots for Light Selective Nanocomposite Thin Films and Solar Cell Applications

Harrison Ward
The University of Western Ontario

Supervisor
Dr. Paul Charpentier
The University of Western Ontario

Graduate Program in Chemical and Biochemical Engineering
A thesis submitted in partial fulfillment of the requirements for the degree in Master of Engineering Science
© Harrison Ward 2016

Abstract

Nanotechnology is allowing the solar energy industry to advance at an accelerating rate, although new materials and processes are required for developing new types of solar cells. Similar to other industries, it is desirable to develop the most environmentally friendly and cost-effective solutions on how to make these next generation materials. Of these new materials, quantum dots (QDs) are of current scientific interest which provide record-breaking increases in efficiency and a new approach for harnessing solar radiation. However, most previous QD work has focused on lead or cadmium based materials, which are not earth friendly and have low thresholds in both California and European legislation. For this reason, this work examines the earth friendly and abundant materials Copper Indium Sulfide (CIS) QDs, i.e. CIS-QDs, which have favorable emission properties. These materials were prepared and examined for use in solar harvesting in photovoltaic (PV) devices.

Copper Indium Sulfide (CIS) QDs were synthesized using three different synthesis techniques, then compared based on their optical and size-dependent properties. Two techniques followed a hydrothermal batch reaction process, referred to as hot injection (HI) and heat up (HU) techniques, that are differentiated by the time at which the sulfur component is added to the reaction medium. The third technique was based on a continuous microfluidic approach. Results showed that the QDs produced from the HU and HI methods have a chalcopyrite structure, with their optical properties being highly dependent on their size and elemental composition. QDs produced from the microfluidic approach were found to agglomerate quickly and had a resulting weak photoluminescent response.

This work examined these QDs in two separate solar applications, both for use in light spectrum conversion with solar films and for use in third generation solar cells. For application in light spectrum conversion, the QDs were melt-mixed with ethylene-vinyl-acetate plastic, using a twin-screw extruder and pressed into thin films using a Carver hydraulic press and Universal film maker. QDs were also reviewed for their use in third

generation solar cell configurations. Based on the optimal configuration, QD sensitized solar cells were fabricated and tested. Resulting current-voltage (IV) curves and solar cell data showed a direct relation between QD composition and cell efficiency.

Key Words: light conversion, ethylene-vinyl acetate, quantum dots, quantum dot solar cells

Acknowledgments

TABLE OF CONTENTS

LIST OF TABLES

LIST OF FIGURES

LIST OF ABBREVIATIONS

AD   average diameter (nm)

CIS   copper indium sulfide

CQD   colloidal quantum dot

DDT   1-dodecanethiol

EVA	ethylene-vinyl acetate copolymer
FTO	fluorine-doped tin oxide
FWHM	full width at half maximum
HI	hot-injection
HU	heat-up
ITO	indium tin oxide
ODE	1-octadecene
QD	quantum dot
QY	quantum yield (%)
SD	standard deviation
SILAR	successive ionic layer absorption and reaction
TEM	transmission electron microscopy
UV	ultra-violet

NOMENCLATURE

A	integrated photoluminescent area
e^-	electron
E_g	band gap
D	quantum dot diameter (nm)
D_B	quantum dot bohr radius
F	absorbance at maximum excitation wavelength

h^+	hole
$h\nu$	light (photon)
$h\nu_{exc}$	excitation light
$h\nu_{pl}$	emission (photoluminescence) light
K_{rad}	energy released from electron transition to k-shell
N	solvent refractive index
Subscript x	refers to unknown sample
Subscript s	refers to known standard

CHAPTER 1: LITERATURE REVIEW

Introduction:

Nanotechnology is a rapidly growing field attracting intense interest across multiple science and engineering disciplines. It has tremendous potential in applications including solar, medical, and various electronic devices (BCC-Research 2008, BCC-Research 2014). Nanotechnology refers to the ability to engineer materials and devices at an atomic scale, typically working with dimensions in the range of 1-100 nm. Advancements in material synthesis techniques and characterization devices has allowed researchers to gain new insight into what is possible using the tools of nanotechnology.

A nanomaterial is defined as any material with at least one dimension limited to the nano–scale, typically less than 100 nm. There are three distinct classifications of nanomaterials: nanosheets, nanorods, and nanodots (W.G.J.H.M. van Sark 2012). A nanosheet is a material with one dimension in the nano-scale, an example being graphene. A nanorod is a material with two quantized dimensions, such as carbon nanotubes, while nanodots, also referred to as quantum dots (QDs), are quantum confined in all three dimensions. Quantum confinement occurs when the diameter of a particle, referred to as 'D' in Figure 1-1, reaches a size smaller than the Bohr radius, D_B, of that material. This causes the energy levels of the material to split, leading to highly tunable electronic and optical properties(W.G.J.H.M. van Sark 2012).
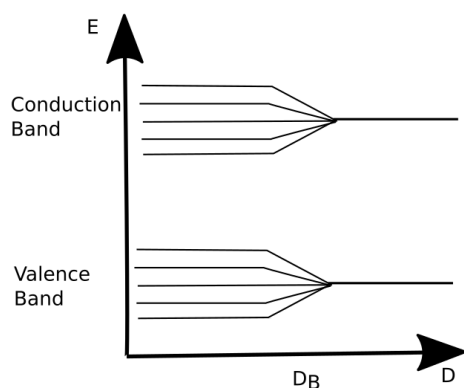
Figure 1-1: Quantum Confinement Effect on Conduction and Valence Band(W.G.J.H.M. van Sark 2012).

All three classifications of nanomaterials have their role in various branches of nanotechnology. QDs are known for their unique ability to selectively convert light energy to different wavelengths, a highly researched process in the solar energy industry (Kamat, 2013).

The start of nanotechnology began in the 1980s with scientists observing molecules at a nano-scale (United States National Nanotechnology Initiative, 2015). The global market for nanomaterials is expected to grow to $64.2 billion by 2019(BCC-Research 2014). The vast majority of this market includes nanoparticles and nano-scale thin films, which accounted for nearly 80% of the nanotechnology market in 2013. From Figure 1-2 it can be seen that solar energy and optoelectronics are experiencing the most rapid growth in recent years. Furthermore, as the population continues to rise, especially in developing countries, global demand for renewable energy will continue to grow, driving the development of new solar energy harvesting technologies.
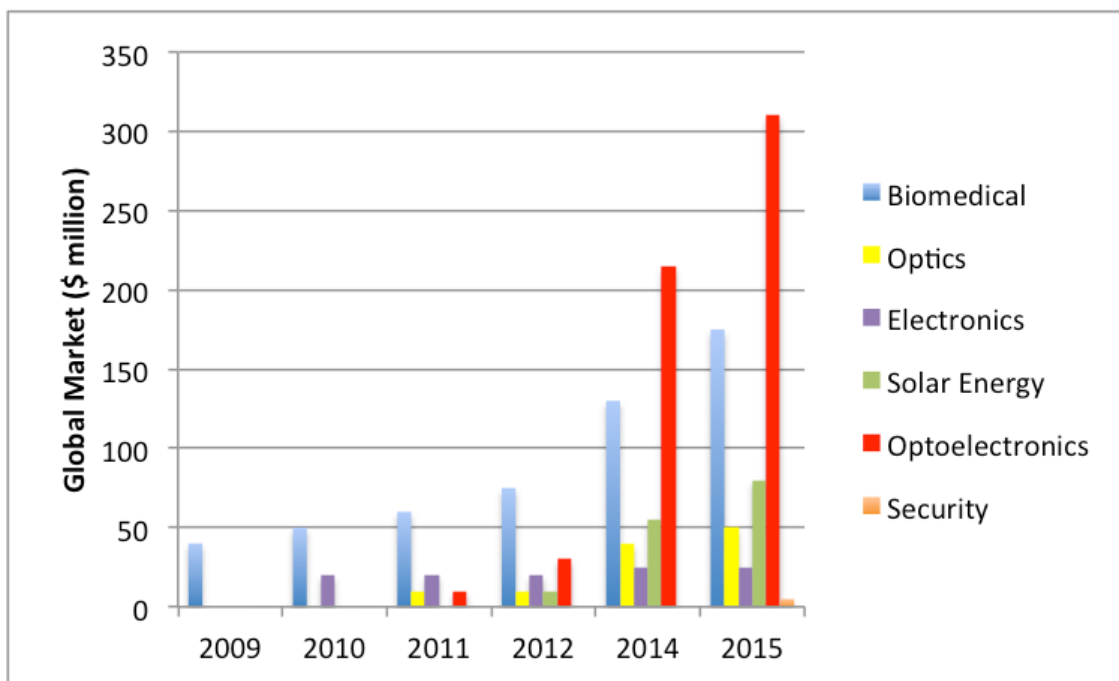
Figure 1-2: Nanotechnology growth in different markets 2009-2015(BCC-Research 2014).

Quantum Dot Classifications:

Quantum dots (QDs) can be organized into three classifications, i.e. core, core-shell, and alloyed QDs (Sigma-Aldrich, 2015). Different materials are used to produce QDs in each of these categories, each with distinct advantages depending on the end-use application. The most commonly used materials for QDs are metal chalcogenides, specifically metal sulfides, selenides, and tellurides. QDs made from elements in groups II-VI and IV-VI, specifically those cadmium and lead based, have attracted the most interest (Kamat 2013, Stolle 2013, Kramer 2014). However any products containing cadmium or lead are hindered by environmental regulations and are not generally accepted by the public. The European Union and California law both restrict the use of cadmium and lead in homogenous materials to 0.01% and 0.1% by weight, respectively (California-Law, 2010 and EUR-Lex, 2011). This has led to the investigation of other elements from group IV and also binary compounds combining elements from groups III and V, such as indium and phosphorous. The most recent research on QDs involves ternary compounds made up of elements from groups I, III, and VI, such as copper, gallium, indium, sulfur, selenium, and tellurium (Guijarro 2014, Pan 2014).
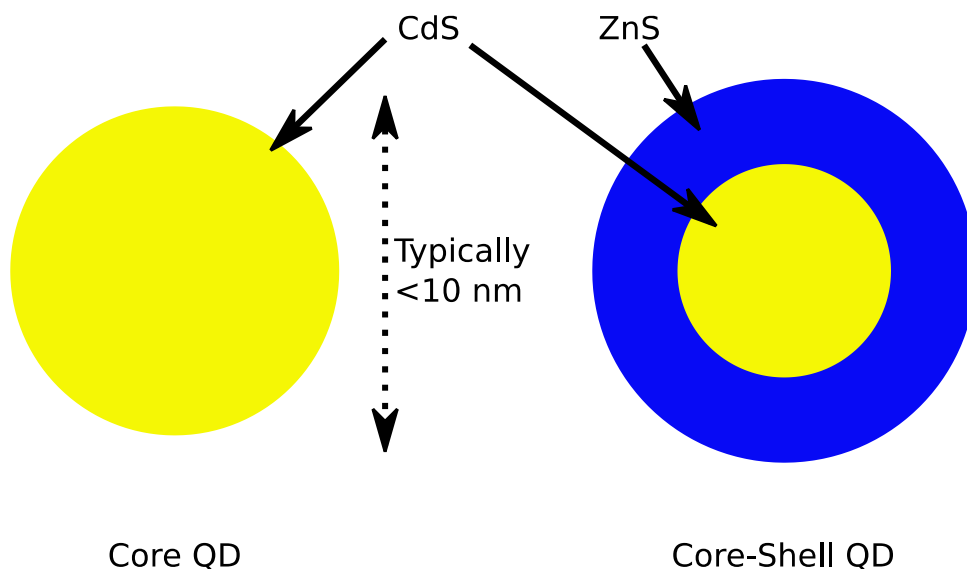
Figure 1-3: Core Vs. Core Shell QDs.

Core Quantum Dots:

The most basic type of QD is referred to as a core QD. Core QDs have a uniform composition and typically consist of two different elements with common examples of core QDs being: CdS, CdSe, CdTe, ZnS, ZnO, PbS, and PbSe. Although these QDs suffer from limited functionality, they are easily tuned by varying their particle sizes (Semonin, Luther et al. 2012, Kamat 2013, Sargent 2013)**.** Cadmium based QDs primarily absorb light in the UV region, while their emission can be tuned across the visible spectrum (Kongkanand, Tvrdy et al. 2008, Lin, Chen et al. 2012). Lead based QDs absorb light from the UV, visible, and near infrared parts of the electromagnetic spectrum. They can be tuned to emit light in the near infrared and infrared parts of the spectrum (Ma, Swisher et al. 2011, Beard, Luther et al. 2013). A strong absorption of light across the majority of the electromagnetic spectrum is attracting researchers' interest for developing solar cells utilizing lead based QDs as the primary absorbing layer (Kramer and Sargent 2014). However, protecting the surrounding environment from exposure to lead remains a current concern, with more environmentally responsible choices necessary.

Core-Shell Quantum Dots:

The fluorescence seen in QDs is a result of electron-hole pairs, also called excitons, recombining through radiative pathways. However, this recombination of charge carriers does not always result in the release of a photon. Instead, this energy can be lost in the form of heat, often caused by distortions in the QD's crystal lattice (G. Ledoux 2001). In order to reduce these heat losses and provide a protective barrier between the QD core and surrounding environment, a different material is used to form the shell layer. By strategically selecting the shell material, the band gap offsets between neighboring materials can be optimized to reduce non-radiative recombination and

maximize effective electron-hole recombination, a process described in Figure 1-4 below.
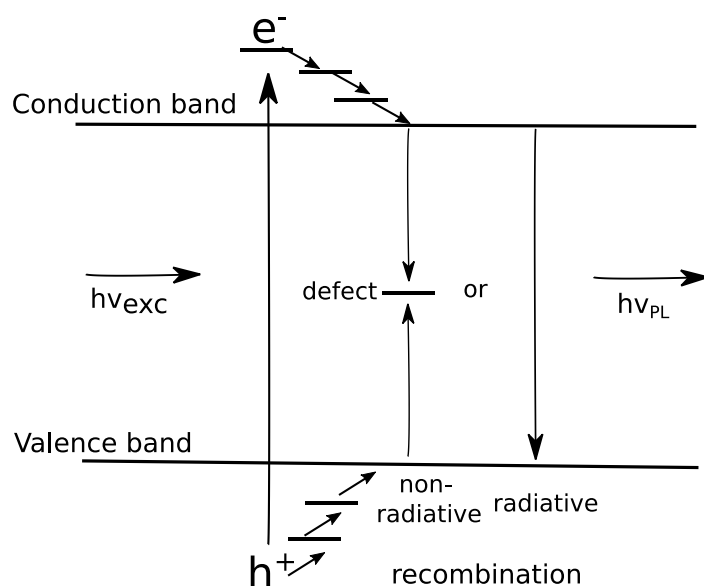
Figure 1-4: Exciton recombination diagram(G. Ledoux 2001).

The effectiveness of a QDs ability to absorb and emit light is their most important feature, which can be quantified by the quantum yield (QY). The QY is defined simply as the ratio of photons emitted to photons absorbed. By coating the QD core material with a different shell material, the QY can be dramatically increased (Sanchez, Binetti et al. 2014).

For QD applications involving light harvesting, it is necessary to position the conduction and valence bands of the core and shell material such that the generated holes remain quantum confined in the core, while electrons remain quantum confined in the shell. This forces the charge carriers to cross the core-shell boundary in order to emit photons, making the process easily tunable by carefully selecting the band gap offset between the individual core and shell materials. To satisfy these conditions, the shell typically requires a higher band gap material than the core (Sanchez, Binetti et al. 2014).

Alloyed Quantum Dots:

Some QD applications, mainly biomedical, have very precise size requirements, making size-controlled tuning of their properties problematic. To overcome this

difficulty, researchers have created alloyed QDs, which are mostly different combinations of the common materials used to produce core and core-shell QDs. Furthermore, the properties of alloyed QDs are distinct from both of their bulk materials and both of their parent semiconductors (Kamat 2013).

CIS Quantum Dots:

Copper-Indium Sulfide (CIS) QDs were chosen in this work for use in QD solar cells and down-conversion because of their relatively low toxicity compared to Cd and Pb, high absorption coefficients, and widely tunable emission wavelength range (McDaniel 2013, Yu 2013). CIS QDs are compatible with a variety of surface ligands and have shown promising results in a variety of applications, including solar, LEDs, and bio-imaging (Song 2012, Yu 2013,Guijarro 2014, and Pan 2014).

Magic Quantum Dots:

QD synthesis typically consists of two main steps, nucleation followed by growth, which causes the products to have a rather broad size distribution. However some researchers have been able to stop the growth process immediately after nucleation. The resulting QDs exhibit highly precise properties and are referred to as magic-sized QDs (Yu, 2010). These QDs are single sized and only exhibit homogenous spectra broadening (Yu, 2010).

Quantum Dot Applications:

The potential applications for QDs continue to grow as new discoveries are made. From Figure 1-2, the current areas of application for QDs can be divided into six categories, i.e., biomedical, optics, electronics, solar energy, optoelectronics, and security. QDs are being used to replace organic dyes in the biomedical industry as fluorescent imaging agents. In the optics industry, QDs are being used to make high performance lasers. QDs are also used in many new electronic versions of cell-phones and televisions. The optoelectronics industry, based on the use of electronic devices to control light, has shown a surge of growth lately. Recent years have shown the emergence of a small

security industry using QD technology mostly for counterfeit applications(BCC-Research 2014). The industry of solar energy utilizing QDs has shown significant growth in recent years and will be an essential requirement to support the growing population's energy demands (BCC-Research 2008, Kamat 2013). This thesis investigates the synthesis of CIS QDs and their application for solar energy harvesting.

Fabrication Methods:

There are a variety of synthesis techniques used to produce QDs. The majority are based on a hydrothermal route, which involves heating up a solution of precursor compounds, organic surfactants, and a solvent. Upon heating, the precursors decompose, forming monomers that initiate crystal growth. The QDs are allowed to grow for a specific amount of time, after which they precipitate from solution. This is traditionally done using either a solvent or anti-solvent wash and then centrifugation in which the QDs are separated from the solvents and reactants by centrifugal force. Recently, new separation techniques have been explored such as using gas-expanded liquids to precipitate the QDs from dispersion(McLeod, Anand et al. 2005). Once the QDs have been recovered, it is then necessary to process them into thin films for use in the end-use application of interest, e.g. photovoltaics. Film deposition is an area attracting significant interest, and is paramount in producing high efficiency solar cells. There are a number of film deposition techniques used today including drop casting or spin coating, chemical bath, successive ionic layer absorption and reaction, electrophoretic deposition, and the use of a molecular linker (Kamat 2013).

The deposition methods for QDs can be split into two categories, those utilizing pre-synthesized QDs and those that grow QDs directly onto a substrate. Pre-synthesized QDs are used in drop casting, spin coating, use of a molecular linker, and electrophoretic deposition techniques. The SILAR process combine both the QD synthesis and film deposition steps into one step using a chemical bath and successive ionic layer absorption and reaction approach. Both approaches have advantages and disadvantages, although research is leading towards the use of pre-synthesized QDs. In the SILAR and chemical

bath approaches, the QD loading is achieved directly onto the metal oxide support, which is most commonly TiO_2. Here the obtained loading is typically higher than that achieved when producing films with pre-synthesized QDs. However recent results from H. Zhang et al. showed 34% coverage of CdSe QDs on TiO_2 films using a molecular linker method (H. Zhang 2012). This value is the highest reported among quantum dot sensitized solar cells (QDSSCs), with typical values being in the range of 14-20%(H. Zhang 2012). Pre-synthesized QDs typically have higher quality and higher QY, and can be easily tuned for specific requirements.

Solar Cell Classifications:

Current solar cell technology can be broken down into five categories: crystalline silicon, which accounts for over 90% of the photovoltaic market in Canada, single junction GaAs, multijunction, thin-film, and emerging photovoltaics, which include QD solar cells (NREL 2014). The highest efficiencies are produced by cells consisting of several different layers of absorbing materials, which are inherently very expensive and only produced on a lab-scale. Crystalline silicon cells dominate the commercial market because of their relatively high efficiency, 15-18% for commercial cells, good stability, and ultimately have the lowest cost/Watt compared to other categories. Thin-film solar cells are referred to as second-generation solar cells, with the goal behind them being to produce very cheap cells to counter their characteristically lower efficiencies. Copper indium gallium selenide/sulfide (CIGS) cells are the dominant technology amongst thin-films and also incorporate nanomaterials in their structure(NREL 2014). CIGS are typically produced using high temperature vacuum deposition methods to achieve uniform film thickness and constant elemental composition. They are deposited onto flexible substrates with the active layer thickness ranging from 1-4 μm, and have reached efficiency's as high as 20.0% (NREL 2014). Based on the proven success of utilizing copper and indium as photoactive materials in CIGS solar cells, copper indium sulfide QDs are a promising strategy for third generation solar cells. The emerging technologies category, is also referred to as third-generation solar cells, which include dye-sensitized

cells (DSSC), perovskite cells, and QD cells. The latter of which is increasing in efficiency at the highest rate amongstst all photovoltaic technologies(NREL, 2014).

Quantum Dot Photovoltaics

There are a number of different approaches to producing solar cells using QDs (Kramer and Sargent 2014). These can be divided into three categories, solid-state heterojunction cells, liquid junction cells, and polymer-QD hybrid cells. Solid-state heterojunction cells can utilize multiple layers of QDs, with each layer capable of absorbing an additional part of the sun's spectrum. This makes them the leading candidate for reaching the highest possible efficiencies. Solid-state cells also avoid degradation from a liquid electrolyte that is used in liquid-junction QD solar cells. Liquid-junction and QD-polymer hybrids have advantages also relating to their structure, processability, and cost (Hines 2014, Lan 2014). QDs can also manipulate solar energy by being combined with traditional silicon-based devices. This is referred to as up and down-conversion.

The architecture of QD solar cells is constantly evolving with new innovations and technologies. The three main categories of QD solar cells: solid-state heterojunction cells, liquid junction cells, and polymer-QD hybrid cells; each have different cell architectures and can be broken down into nine groups. The record efficiency for each classification can be seen below in Table 1-1.

Table 1-1: Record efficiencies of different QD solar cell designs(Kramer and Sargent 2014).

Configuration	Efficiency (%)
Colloidal QDSSC	5.4
QDSSC (substrate growth such as CBD or SILAR)	5.6
Schottky	4.6
Depleted heterojunction	8.5
Depleted bulk heterojunction	7.3
Bulk-nano heterojunction	4.9
Quantum junction	7.4
Multijunction	4.2

Colloidal Quantum Dot Sensitized Solar Cell:

This type of configuration is very similar to a dye-sensitized solar cell with the dye being replaced by colloidal QDs. The first time a solar cell of this nature was reported was in 1998 utilizing InP QDs as sensitizers (Zaban, 1998). This type of cell includes a monolayer coating of colloidal QDs over a transparent, nanoporous electron acceptor like TiO_2 or ZnO. This interface is then permeated with a liquid electrolyte, commonly an organic polysulfide, for hole collection. A primary challenge with these types of solar cells is achieving continuous, monolayer coverage of the entire nanoporous electron acceptor. This can be attributed to the colloidal QD diameter being much larger than the nanoporous TiO_2 pore diameter. Poor coverage of the electron-accepting layer leads to it coming into direct contact with the hole-transporting electrolyte. This leads to back injection of the charge carriers, which significantly degrades device performance.

In an effort to overcome this issue, researchers are depositing a higher band gap layer, commonly ZnS, overtop of the QD layer to prevent contact with the electrolyte(Guijarro, Guillen et al. 2014). An alternative approach involves sensitizing solution stable TiO_2 nanoparticles with the QDs prior to film deposition of the QD – TiO_2 nanostructure. Although efficiencies of greater than 5% have been successfully demonstrated with this approach, using a chemical bath deposition or SILAR method allows for QD synthesis and film deposition to be carried out in a single step (Zhang, 2012). This provides some advantages for QD coverage, but not without sacrificing optical properties and monodispersity(Kramer and Sargent 2014).

The operating principle of a QDSSC is very similar to that of a DSSC. When the QDs absorb a photon with high enough energy, they promote an electron to its conduction band. This electron is then injected into the conduction band of nanoporous TiO_2. At the same time the hole resulting from the electron that was excited to the conduction band of the QDs is transported into the liquid electrolyte, where it undergoes reduction. The electron travelling through the TiO_2 passes through the anode and then reenters the cell through the cathode, creating an electrical current(Kamat 2014).

Schottky Colloidal Quantum Dot Solar Cell:

These types of cells rely on an electron affinity difference between the top, a transparent conductive oxide, and the back, commonly Mg or Al, contact layers of the cell(Kramer and Sargent 2014). This produces a built-in electric field, which acts as the driving force for extraction of electrons and holes. These cells typically utilize PbS QDs for electron extraction that are blended with an organic polymer, which facilitates hole extraction. The first cell with this architecture was produced in 2005 (McDonald, 2005). After extensive investigation into the polymer's impact on electrical properties, it was found to actually hinder hole extraction, compared to the improved hole transport in QDs themselves. By producing these devices without a polymer component, it was confirmed that with an electric field, thin-films consisting of only QDs could effectively separate and transport both electrons and holes. This made Schottky QD solar cells more similar to polycrystalline thin-film cells, with the major advantage of having quantum-tuned band gaps(Kramer and Sargent 2014).

Schottky cells are attractive because of their functional simplicity, ease of fabrication, excellent potential for mass production using a roll-to-roll process, and good demonstration of the stand-alone ability of QD thin-films (Luther, 2008). These have reached efficiencies greater than 4.5%(Ma, Swisher et al. 2011).

The architecture of a polymer-QD hybrid solar cell is similar to the solid-state heterojunction cell. It consists of conductive and transparent anode layer, commonly ITO or FTO, then the photoactive layer, which is a combination of the polymer material and QDs, and finally the cathode layer, commonly aluminum(Ma, Swisher et al. 2011).

Depleted Heterojunction:

The idea behind a depleted heterojunction QD solar cell is to combine the advantages of the Schottky and QDSSCs (Pattantyus-Abraham, 2010). This type of cell consists of a transparent anode, commonly FTO or ITO on glass. A wide band gap

semiconductor is deposited on top, commonly TiO_2 or ZnO, which does not have to be nanoporous. Next the QD active layer is deposited onto the wide band gap semiconductor, with a thickness of 50-300nm(Kramer and Sargent 2014).

Selection of appropriate surface ligands is critical in depleted heterojunction cells in order to achieve the best interfacial contact between the QD active layer and wide band gap semiconductor transport layer. Tuning conduction band offsets is of critical importance as improperly matched band gaps of two different materials at an interface creates a barrier for electron injection. By carefully controlling the band offsets, efficient charge extraction can occur without a strong electric field (Kramer and Sargent 2014). Optimization of band gap offsets through careful selection of QD size has produced efficiencies as high as 8.5% (Maraghechi, 2013).

Depleted bulk heterojunction, bulk-nano heterojunction, quantum junction, and multijunction cells are all similar to the depleted heterojunction cell in design, with minor differences in the materials used. These types of cells can all be classified as solid-state heterojunction cells.

Down-Conversion:

QDs can also be applied to existing solar cell technologies, primarily silicon based cells, to increase efficiency. One of these concepts is referred to as down-conversion. This is a process during which the QDs convert a portion of the sun's electromagnetic spectrum, that was previously unutilized high-energy UV light, into wavelengths more suited for absorption using a traditional solar cell. The QDs can be combined with a protective polymer and applied as the top lamination layer on silicon solar cells. QDs can be fine tuned to emit light at the band gap energy of the silicon absorbing layer and provide significant increases in efficiency. This strategy is also desirable because it minimizes costs associated with establishing a new commercial manufacturing process, something that would be required for the other QD solar cell technologies discussed above.

Down-conversion refers to the process where a single high-energy photon is converted to multiple lower energy photons. Essentially this process is capable of concentrating the sun's light spectrum into narrower, high intensity spectrums, with the tunable emission wavelength dependent on the final application. This also reduces thermalization loses in first generation solar cells, through a concept referred to a multiple exciton generation (MEG) (NREL 2012). Two similar processes also attracting researchers' attention are down shifting, a less efficient form of down-conversion, and up conversion, the exact opposite process of down-conversion.
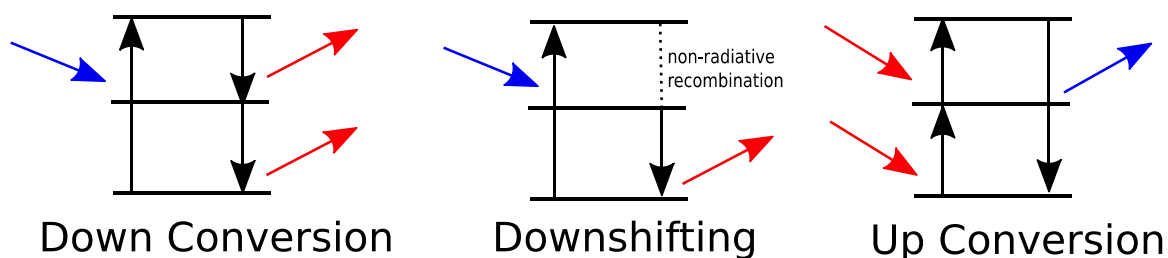
Figure 1-5: Light Converting Mechanisms (W.G.J.H.M. van Sark 2012).

MEG is a phenomenon unique to QDs. Traditionally the absorption of a photon causes a single electron to jump from the valence band to the conduction band. If the energy of the photon is higher than that of the absorbing material's band gap, it is released in the form of heat, also referred to as a thermalization loss. When QDs absorb photons with energy's higher than their band gap, the energy can be exchanged between multiple electrons, leading to the formation of multiple electron-hole pairs or excitons. This process is described in Figure 1-6.
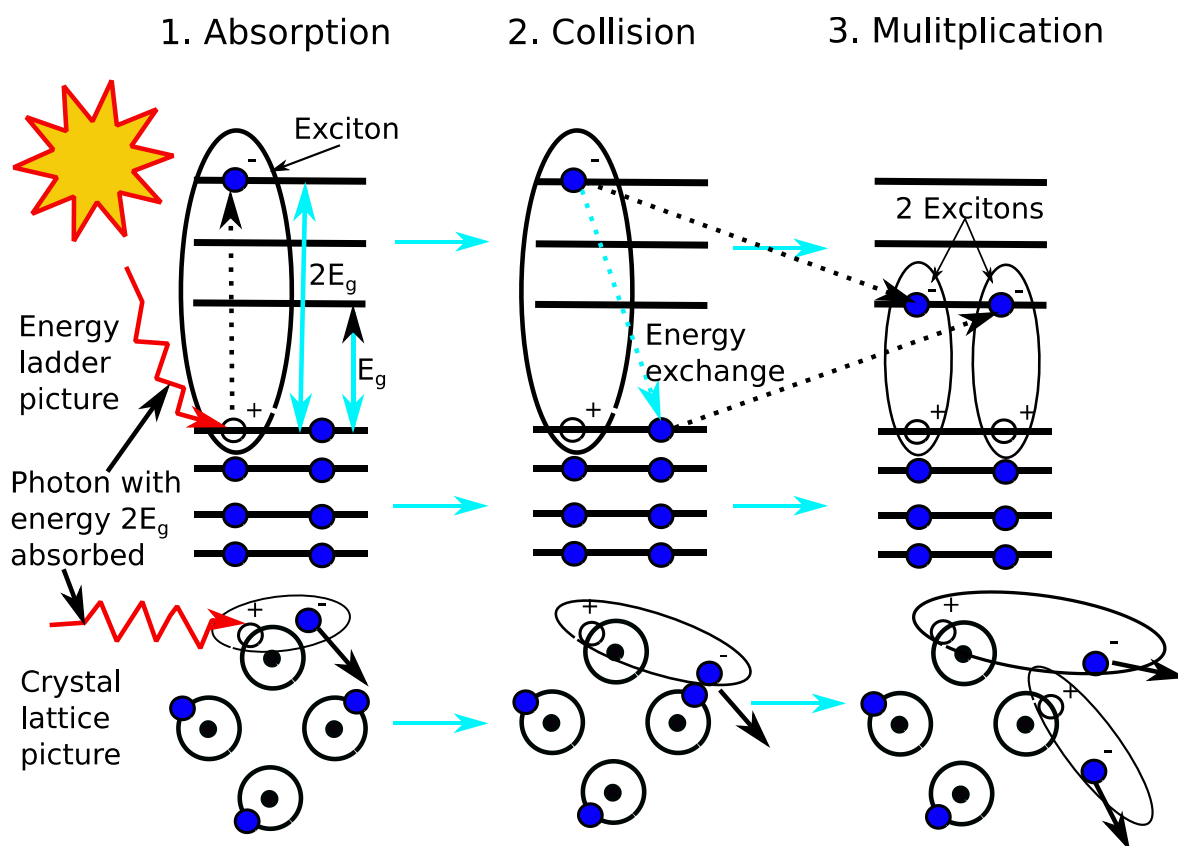
Figure 1-6: Schematic of MEG Mechanism (NREL 2012)

Very few reports have been published on these concepts. There have been some studies on the use of rare earth ions for up-conversion and the use of nano-layered zinc oxide as a down-conversion layer (Yao Zhu 2013, SISER 2014). However there are no studies available on the use of CIS QDs as a down converting layer.

Technology Classification:

The seven different QD solar cell configurations discussed above can be organized into three distinct categories.

Table 1-2: QD Solar Cell Classifications

Classification	Configurations
Solid-State Heterojunction	Depleted Heterojunction, Depleted Bulk Heterojunction, Bulk-Nano

	Heterojunction, Quantum Junction, and Multijunction
Liquid-Junction	QDSSC
QD-Polymer Hybrid	Schottky

The majority of researchers working with QDs synthesize them in their own labs, as there are only a few commercial suppliers of QDs. However, the cost for these QDs is currently very high and varies substantially from supplier to supplier. This is because of the wide variety in quality, composition, manufacturing processes, and geographical location between the suppliers. QDs are a specialty chemical and the only prices available for them are from companies selling them for research purposes. These costs also have to cover the extensive QD product characterization required by the company to insure they provide a consistent, premium product. Large chemical companies are currently pursuing partnerships with companies that have expertise in QD manufacturing at a smaller scale in hopes of gaining control of the emerging commercial market for QDs. This will lead to a significant reduction in cost and more widespread availability.

Table 1-3: Cost comparison of commercial QDs (Crystalplex 2014, Mesolight 2014, Nanotech 2014, Sigma-Aldrich 2014)

Supplier	Cost per 50 mg
Crystalplex	$500-700
Mesolight	$200-600
Ocean Nanotech	$250-900
Sigma Aldrich	$500-1000

Future of QD Solar Applications

QDs are allowing for progression of the photovoltaic industry at an impressive rate. The growth rate of investment for QDs used in solar and other applications can be seen in Figure 1-7. As new techniques for improving surface chemistry, interface interactions, and new materials for QD solar cells appear in research, they will continue to press records in efficiency and help support the growing global demand for renewable

energy. Some of the more important areas requiring improvements for economic commercialization are in synthesis techniques such as continuous production using a microfluidic reactor system. Incorporating roll-to-roll processing techniques for QD solar cells will also be critical in achieving commercial feasibility.
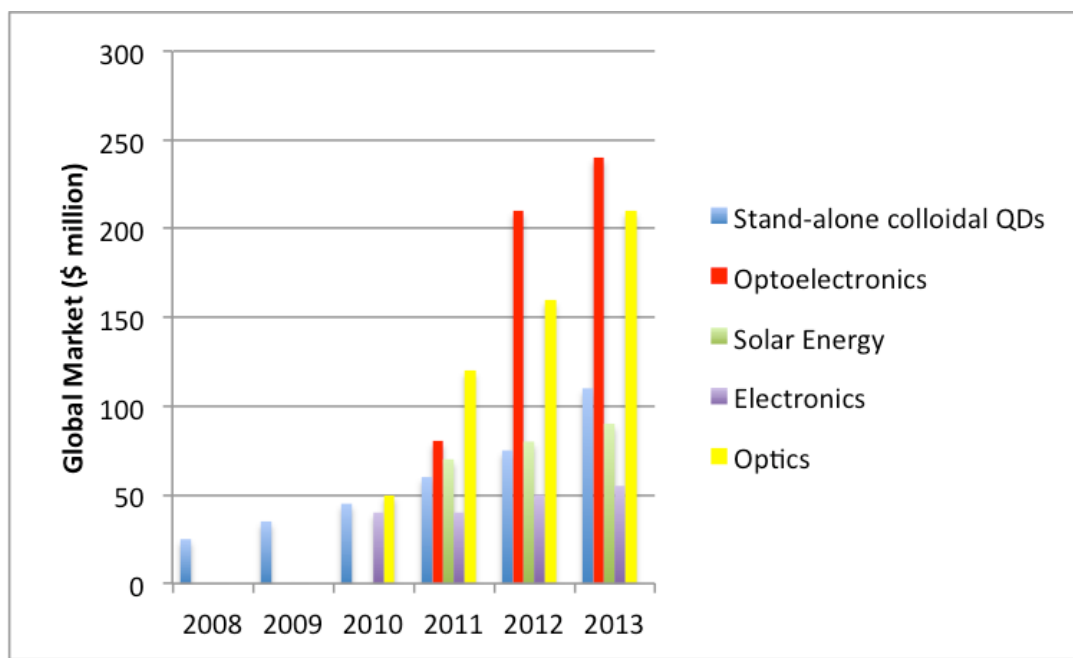
Figure 1-7: QD Market Growth 2008-2013(BCC-Research 2008)

OBJECTIVES:

The objectives of this thesis were to:

1. Evaluate available synthesis methods for producing non-cadmium or lead free quantum dots, focusing on copper indium sulfide.
2. Investigate the use of these quantum dots in polymer films for application as a light-selective thin film using downregulation.
3. Investigate the use of these quantum dots as the primary absorbing layer in a quantum dot solar cell design.

Bibliography

1. Barkhouse, D. A. R., Debnath, R., Kramer, I. J., Zhitomirsky, D., Pattantyus-Abraham, A. G., Levina, L., Etgar, L., Grätzel, M. and Sargent, E. H. "Depleted Bulk Heterojunction Colloidal Quantum Dot Photovoltaics." Advanced Materials. 2011, 23, 3134.

2. BCC-Research (2008). Quantum Dots: Technical Status and Market Prospects. Wellesley, MA.

3. BCC-Research (2014). Quantum Dots: Global Market Growth and Future Commercial Prospects. London England.

4. Beard, M. C., J. M. Luther, O. E. Semonin and A. J. Nozik (2013). "Third generation photovoltaics based on multiple exciton generation in quantum confined semiconductors." AccChem Res 46(6): 1252-1260.

5. British-Petroleum (2014). BP Energy Outlook 2035. London England.

6. California-Law. (2010). "What are the Maximum Containment Values (MCVs) for these Metals in Products." from https://www.dtsc.ca.gov/HazardousWaste/rohs2_MCVs.cfm.

7. Crystalplex. (2014). "Crystalplex Quantum Dots, Semiconductor Nanocrystals." 2014, from http://www.crystalplex.com/SearchResults.asp?Cat=1.

8. EUR-Lex (2011). COMMISSION DIRECTIVE 2011/37/EU. EUR-Lex: Access to European Union Law, Official Journal of the European Union.

9. G. Ledoux, O. G., F. Huisken, B. Kohn, D. Porterat and C. Reynaud (2001). "Crystalline silicon nanoparticles as carriers for the Extended Red Emission." Astronomy and Astrophysics 377: 707-720.

10. Group, W. R. (2012). "Lead-salt Semiconductor Quantum Dots." 2015, from http://wise.research.engineering.cornell.edu/index.html.

11. Guijarro, N., E. Guillen, T. Lana-Villarreal and R. Gomez (2014). "Quantum dot-sensitized solar cells based on directly adsorbed zinc copper indium sulfide colloids." PhysChemChemPhys 16(19): 9115-9122.

12. Gur, I.,Fromer, N., Geier, M., Alivisatos, A. "Air-stable all-inorganic nanocrystal solar cells processed from solution." Science. 2005, 310, 462.

13. H. Chung, a. P. H. H. (2007). "Phosphor coatings to enhance Si photovoltaic cell performance." Journal of Vacuum Science and Technology 25: 61-66.

14. H. Zhang, K. C. (2012). "Efficient CdSe quantum dot-sensitized solar cells prepared by a postsynthesis assembly approach." Chemical Communication 48: 11235-11237.

15. Hines, D. A. and P. V. Kamat (2014). "Recent advances in quantum dot surface chemistry." ACS Appl Mater Interfaces 6(5): 3041-3057.

16. Kamat, P. V. (2013). "Quantum Dot Solar Cells.The Next Big Thingin Photovoltaics." The Journal of Physical Chemistry Letters 4(6): 908-918.

17. Katsuhiro Nose, T. O., and Shinya Otsuka-Yao-Matsuo (2008). "Colloidal Synthesis of Ternary Copper Indium Diselenide Quantum Dots and Their OpticalProperties." Journal of Physical Chemistry 113: 3455-3460.

18. Kongkanand, A., K. Tvrdy, K. Takechi, M. Kuno and P. V. Kamat (2008). "Quantum dot solar cells. Tuning photoresponse through size and shape control of CdSe-TiO2 architecture." J Am ChemSoc 130(12): 4007-4015.

19. Kramer, I. J., Zhitomirsky, D., Bass, J. D., Rice, P. M., Topuria, T., Krupp, L., Thon, S. M., Ip, A. H., Debnath, R., Kim, H.-C. and Sargent, E. H. "Ordered Nanopillar Structured Electrodes for Depleted Bulk Heterojunction Colloidal Quantum Dot Solar Cells." Advanced Materials. 2012, 24, 2315.

20. Kramer, I. J. and E. H. Sargent (2014). "The architecture of colloidal quantum dot solar cells: materials to devices." Chem Rev 114(1): 863-882.

21. Lan, X., S. Masala and E. H. Sargent (2014). "Charge-extraction strategies for colloidal quantum dot photovoltaics." Nat Mater 13(3): 233-240.

22. Leschkies, K., Jacobs, A., Norris, D., Aydil, F. "Nanowire-quantum-dot solar cells and the influence of nanowire length on the charge collection efficiency." Applied Physics Letters. 2009, 95, 193103.

23. Liu, H., Tang, J., Kramer, I. J., Debnath, R., Koleilat, G. I., Wang, X., Fisher, A., Li, R., Brzozowski, L., Levina, L. and Sargent, E. H. "Electron Acceptor Materials Engineering in Colloidal Quantum Dot Solar Cells." Advanced Materials. 2011, 23, 3832.

24. Luther, J., Law, M., Beard, M., Song, Q., Reese, M., Ellingson, R. and Nozik, A. "Schottky Solar Cells Based on Colloidal Nanocrystal Films". Nano Letters. 2008, 8, 3488.

25. Ma, W., S. L. Swisher, T. Ewers, J. Engel, V. E. Ferry, H. A. Atwater and A. P. Alivisatos (2011). "Photovoltaic performance of ultrasmallPbSe quantum dots." ACS Nano 5(10): 8140-8147.

26. Maraghechi, P., A. J. Labelle, A. R. Kirmani, X. Lan, M. M. Adachi, S. M. Thon, S. Hoogland, A. Lee, Z. Ning, A. Fischer, A. Amassian and E. H. Sargent (2013). "The donor-supply electrode enhances performance in colloidal quantum dot solar cells." ACS Nano 7(7): 6111-6116.

27. McDaniel, H., N. Fuke, N. S. Makarov, J. M. Pietryga and V. I. Klimov (2013). "An integrated approach to realizing high-performance liquid-junction quantum dot sensitized solar cells." Nat Commun 4: 2887.

28. McDonald, S., Konstantatos, G., Zhang, S., Cyr, P., Klem, E., Levina, L. and Sargent, E. "Solution-processed PbS quantum dot infrared photodetectors and photovoltaics." Nature Materials. 2005, 4, 138.

29. McLeod, M. C., M. Anand, C. L. Kitchens and C. B. Roberts (2005). "Precise and rapid size selection and targeted deposition of nanoparticle populations using CO2 gas expanded liquids." Nano Lett 5(3): 461-465.

30. Mesolight. (2014). "Quantum Dot Products." from http://www.mesolight.com/index.php.

31. Nanoco-Group-PLC. (2014). "Quantum Dots manufactured in Bulk Quantities." 2014, from http://www.nanocotechnologies.com/index.aspx.

32. Nanotech, O. (2014). "Products Catalogue ", from http://www.oceannanotech.com/catalog.php.

33. Ning, Z., D. Zhitomirsky, V. Adinolfi, B. Sutherland, J. Xu, O. Voznyy, P. Maraghechi, X. Lan, S. Hoogland, Y. Ren and E. H. Sargent (2013). "Graded doping for enhanced colloidal quantum dot photovoltaics." Adv Mater 25(12): 1719-1723.

34. NREL. (2012). "Novel Physical Principles Research Thrust." 2015, from http://www.centerforadvancedsolarphotophysics.org/physical_principles.html.

35. NREL. (2014). "National Center for Photovoltaics." 2015, from http://www.nrel.gov/ncpv/.

36. Pan, Z., I. Mora-Sero, Q. Shen, H. Zhang, Y. Li, K. Zhao, J. Wang, X. Zhong and J. Bisquert (2014). "High-efficiency "green" quantum dot solar cells." J Am ChemSoc 136(25): 9203-9210.

37. Pattantyus-Abraham, A.,Kramer, I., Barkhouse, A., Wang, X., Konstantatos, G., Debnath, R., Levina, L., Raabe, I., Nazeeruddin, M., Grätzel, M. and Sargent, E. "Depleted-Heterojunction Colloidal Quantum Dot Solar Cells". ACS Nano. 2010, 4, 3374.

38. Queisser, W. S. a. H. J. (1961). "Detailed Balance Limit of Efficiency of p- n Junction Solar Cells." Journal of Applied Physics 32: 510-519.

39. Sanchez, R. S., E. Binetti, J. A. Torre, G. Garcia-Belmonte, M. Striccoli and I. Mora-Sero (2014). "All solution processed low turn-on voltage near infrared LEDs based on core-shell PbS-CdS quantum dots with inverted device structure." Nanoscale 6(15): 8551-8555.

40. Sargent, G. K. a. E. H. (2013). Colloidal Quantum Dot Optoelectronics and Photovoltaics Cambridge, Cambridge University Press.

41. Semonin, O. E., J. M. Luther and M. C. Beard (2012). "Quantum dots for next-generation photovoltaics." Materials Today 15(11): 508-515.

42. Sigma-Aldrich. (2014). "Quantum Dots - Products." from http://www.sigmaaldrich.com/materials-science/material-science-products.html?TablePage=16376883.

43. Sigma-Aldrich. (2015). "Quantum Dots." from http://www.sigmaaldrich.com/materials-science/nanomaterials/quantum-dots.html

44. SISER. (2014). "Up and Down-conversion." from http://siser.eps.hw.ac.uk/research/next-generation/up-and-down-conversion.

45. Song, W.-S. and H. Yang (2012). "Efficient White-Light-Emitting Diodes Fabricated from Highly Fluorescent Copper Indium Sulfide Core/Shell Quantum Dots." Chemistry of Materials 24(10): 1961-1967.

46. Stolle, C. J., T. B. Harvey and B. A. Korgel (2013). "Nanocrystal photovoltaics: a review of recent progress." Current Opinion in Chemical Engineering 2(2): 160-167.

47. Sungwoo Kim, M. K., Seajin Kim, Jin-HyukHeo, Jun Hong Noh, Sang HyukIm, Sang IlSeok, and Sang-Wook Kim (2013). "Fabrication of CuInTe2 and CuInTe2xSex Ternary Gradient Quantum Dots and Their Application to Solar Cells." ACS Nano.

48. United States National Nanotechnogy Initiative. (2015). "Nanotechnology Timeline." Retrieved March 30, 2015, from http://www.nano.gov/timeline.

49. W.G.J.H.M. van Sark, A. M. a. R. E. I. S. (2012). Solar Spectrum Conversion for Photovoltaics Using Nanoparticles. Third Generation Photovoltaics. D. V. Fthenakis, INTECH.

50. Yang, J., J. Y. Kim, J. H. Yu, T. Y. Ahn, H. Lee, T. S. Choi, Y. W. Kim, J. Joo, M. J. Ko and T. Hyeon (2013). "Copper-indium-selenide quantum dot-sensitized solar cells." PhysChemChemPhys 15(47): 20517-20525.

51. Yao Zhu, A. A., Bruno Masenelli and Patrice Melinon (2013). "Zinc oxide nanoparticles as luminescent down-shifting layer for solar cells." SPIE.

52. Yu, K., Hu, M., and Wang, R., Piolet, M., Frotey, M., Zaman, M., Wu, X., Leek, D., Tao, Y., Wilkinson, D., and Li, C. "Thermodynamic Equilibrium-Driven Formation of Single-Sized Nanocrystals: Reaction Media Tuning CdSe Magic-Sized versus Regular Quantum Dots." J. Phys. Chem. C, 2010, 114 (8), pp 3329–3339.

53. Zaban, A. M., O. I.; Gregg B. A.; Nozik A. J. (1998). "Photosensitization of Nanoporous TiO2 Electrodes with InP Quantum Dots." Langmuir**14**(3153-3156).

54. Zhang, H., Cheng, K. (2012). "Efficient CdSe quantum dot-sensitized solar cells prepared by a postsynthesis assembly approach." Chemical Communication 48: 11235-11237.

55. Zhitomirsky, D., Furukawa, M., Tang, J., Stadler, P., Hoogland, S., Voznyy, O., Liu, H. and Sargent, E. H. "N-Type Colloidal-Quantum-Dot Solids for Photovoltaics." Advanced. Materials. 2012, 24, 6181.

CHAPTER 2: SYNTHESIS OF COPPER INDIUM SULFIDE QUANTUM DOTS FOR USE IN QUANTUM DOT SENSITIZED SOLAR CELLS

Abstract:

Third generation solar cells utilize high-performance high-cost nanomaterials, termed quantum dots (QDs), capable of reaching high efficiencies. Specifically QDs can be used in place of organic dyes in a cell configuration similar to that of the well-known dye-sensitized solar cell (DSSC) design. QDs exhibit higher absorption coefficients and increased tunability compared to organic dyes. However most QDs utilize lead or cadmium, which are not considered earth friendly elements. Copper indium sulfide (CIS) QDs are of interest, but the relationship between structure and properties is unknown.

This work examines three alternative techniques for the synthesis of CIS QDs. Two are based on hydrothermal synthesis procedures while the third compares a novel microfluidic reactor system approach. The resulting QD samples were characterized based on their optical, size-dependent and structural properties. The effectiveness of each approach was determined by comparing the quantum yields and size distributions of synthesized samples. Experimental results revealed that QD samples with lower monodispersity gave higher quantum yields. Then, solar cells utilizing CIS QDs as the primary absorbing layer were fabricated and tested. Cell performance was found to be highly dependent on the QD composition and dramatically increase with the use of a passivation layer.

Introduction:

Quantum Dots (QDs) are quickly emerging as the next major technology in the solar industry (Stolle 2013). They provide unique properties that can be easily manipulated to suit specific application requirements. QDs were first discovered in the early 1980s and have been attracting a surge of interest related to their application in photovoltaics in the last ten years(Kamat 2013). While group II−VI and IV−VI cadmium- or lead-based QDs have been the focus of greatest interest, other materials such as group I−III−VI semiconductors combining group I (Cu, Ag), group III (Al, Ga, In, Tl), and group VI (S, Se, Te) elements have been identified as potentially less toxic materials. Products containing cadmium or lead are hindered by environmental regulations, e.g. the European Union and California both restrict the use of cadmium and lead in homogenous materials to 0.01% and 0.1% by weight, respectively (California-Law, 2010 and EUR-Lex, 2011). Considering the quantum confinement effects, QDs of I−III−VI semiconductors cover a broad range of optical and electronic properties with tunable band gaps covering a wide wavelength range from the near-infrared region, through visible, to the UV region(H. Zhang 2012). This makes CIS QDs an excellent candidate for use in solar applications.

Similar to other renewable technologies, the bottleneck for QD photovoltaics is with the economy of scale involved in their production. The chemistry involved during crystal nucleation is difficult to control, making large-scale production challenging (Chang and Waclawik 2013 and Hines 2013). There have been a number of different techniques used in the literature to synthesize QDs, most of which rely on a hydrothermal reaction of metal salts in a high boiling point solvent. Although this procedure can produce high quality QDs, it has several drawbacks, including batch mode operation, long residence times, and requires vacuum and/or inert gas for the reaction to take place (Hines and Kamat 2014).

This work examines three different approaches for synthesizing CIS QDs. The first two techniques are based on approaches most commonly used in the literature and

the third is a novel microfluidic synthesis method. The methods most commonly reported in the literature can be organized into two classifications, hot-injection (HI) and heat-up (HU) techniques. Both techniques involve preparing a precursor solution of copper and indium salts in a non-polar solvent, with or without the addition of a surfactant (Yang, Kim et al. 2013, Yu, Ng et al. 2013, PB Kreider 2014). This work provides new insight on the relationship between synthesis methods and the quantum yield and size distribution of QD products. In the case of the HU technique, a sulfur-containing compound is also added to the precursor solution prior to heating (Chang and Waclawik 2013). The reaction solution at room temperature is then heated up under vacuum, to between 180 and 320 °C, which is then maintained for as little as 5 minutes or up to several hours, depending on the other synthesis parameters. The reaction solution is constantly mixed using a magnetic stir bar set to a moderately high mixing speed. Due to the continuous flow in the microfluidic system, additional mechanical mixing is not required. For the HI technique, the reaction is initiated by injecting the sulfur-containing compound into the reaction solution once it has reached sufficient temperature. The reaction chemistry in this approach is very complex and has still not been thoroughly explained in literature, however, it has been shown that HI methods produce a more narrow size distribution of particles, due to a more constant growth temperature (Kamat 2013 and Sungwoo 2013).
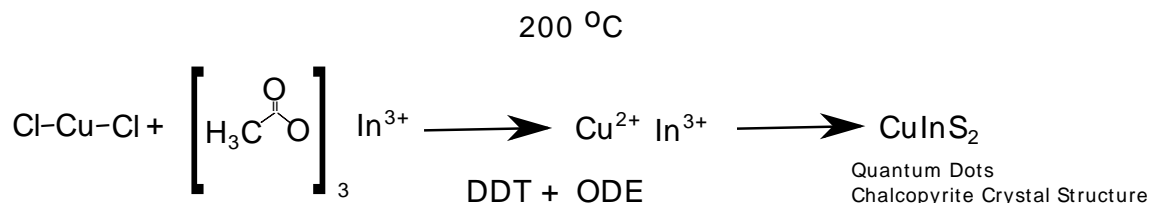
Figure 2-1: Reaction schematic for formation of CIS QDs from copper (II) chloride and indium (III) acetate (Chang and Waclawik 2013).

There are many factors that contribute to the surface chemistry of QDs. The properties of QDs are highly dependent on surface chemistry, making it crucial to control. However this can be difficult because there is still so much unknown on QD chemistry. The KAMAT lab (Kamat 2014) has performed studies showing the effect of washing procedures, quenching time, and storage conditions on QDs (Hines and Kamat 2014). With so many factors able to affect the QD product, it is essential to maintain precise

conditions during the experiments. Many methods in the literature use highly toxic surfactants such as tri-octylamine. With the goal of this work being to reduce the toxicity of the QDs used, it is also desirable to have a synthesis method using green chemistry. The surfactant used for the majority of this work was 1-dodecanethiol, which is also the sulfur source for the reaction and functional ligand for QD applications.

The optimized QD synthesis procedure used octadecene as the reaction solvent, 1-dodecantethiol as the sulfur source and surface ligand, copper (II) chloride and indium (III) acetate as the precursors. QD synthesis techniques, including precursor ratios used, were adapted from several methods reported in literature(Yang, Kim et al. 2013, Yu, Ng et al. 2013, PB Kreider 2014). Batch synthesis procedures based on HI and HU methods were explored as well as a continuous-flow synthesis approach. The microfluidic reactor allows for an increased rate of heat transfer due to the small diameter and high surface area of the tubing exposed to the heat source. This reduces the amount of time required for crystal nucleation to take place, the rate limiting step in quantum dot formation. All batch methods included the use of a non-polar solvent, organic surfactant, and metal salt precursors. As shown by the Jensen group at MIT, the benefits of using a microfluidic reactor for QD synthesis are potentially an improved reaction yield, continuous production and easy scale-up, increased QY, decreased particle size distribution, and improved life cycle analysis (Jensen 2009). QDs can be produced in less than 5 minutes and require substantially less energy input. The microfluidic reactors used by the Jensen Group make use of specifically designed microfluidic cells that allow extremely precise control over reaction conditions, compared to the more simple design of the microfluidic reaction system used in this work.

Experimental Section:

Materials:

Copper (II) chloride ($CuCl_2$, 99.995%, Sigma Aldrich), indium (III) acetate ($In(C_2H_3O_2)_3$, 99.99%, Sigma Aldrich), 1-dodecanethiol ($CH_3(CH_2)_{11}SH$, 98%, Sigma Aldrich), and 1-octadecene ($CH_3(CH_2)_{15}CH=CH_2$, 90%,Sigma Aldrich) were used without further

purification. Anhydrous methanol (99.8%) and toluene (99.9%, CHROMASOLV Plus) were purchased from Sigma Aldrich and used as received.

Electrolyte (Iodolyte Z-150, 150 mM iodide/triiodide in 3 methoxypropionitrile, Solaronix 35321), counter electrode (test cell platinum electrode, Solaronix 74201), electrode (test cell transparent titania electrode, Solaranix 74111), CIS QDs (from HU method), dichloromethane (CH_2Cl_2, 99.5%, Sigma Aldrich), zinc acetate(($CH_3CO_2)_2Zn$, 99.99%, Sigma Aldrich), and sodium sulfide (Na_2S, Sigma Aldrich) were used without further purification.

Heat-Up Synthesis Method:

In this synthesis method, the precursor powders, 0.2 mmol copper (II) chloride and 0.4 mmol indium (III) acetate were combined in a three-neck reaction flask with the solvent, 10 mL 1-octadecene, and surfactant, 1.5 mL 1-dodecanethiol, at room temperature. The flask was then drawn under vacuum and heated to 80°C. It was maintained with magnetic stirring until all bubbling stopped, about 30-60 minutes. The flask was then heated to 200 °C and maintained under vacuum while the crystal nucleation and growth took place (10-120 minute reaction were examined). The flask was allowed to cool to room temperature, with a subsequent addition of a non-polar solvent such as chloroform or toluene to help disperse the QD particles, followed by addition of a polar solvent, methanol to precipitate the QD particles. The suspension was centrifuged at 6000 rpm for 10 minutes, with the supernatant being discarded and the QD precipitate being dispersed in toluene, followed by addition of methanol before centrifuging again at 6000 rpm for 10 minutes. This washing process was repeated at least twice to ensure the final product was free of unreacted precursors. The QD powder was then dried overnight in a vacuum oven at 80 °C.

Hot-Injection Synthesis Method:

This methodology is similar to the HU method, however it involved heating up the precursor solutions separately prior to the QD reaction. The metal salt precursors, copper

(II) chloride and indium (III) acetate, were combined in one flask with 10 mL of 1-octadecene and heated up to 200 ºC under vacuum, while the sulfur-containing surfactant (1.5 mL of 1-dodecanethiol) was heated up to a similar temperature and then injected into the metal salt solution once it reached 200 ºC. The injection was carried out rapidly, typically lasting about 10 seconds.

Microfluidic Synthesis Method:

The synthesis process involved two main steps. Precursor mixing followed by controlled crystal growth. First the metal salt precursors, copper (II) chloride and indium (III) acetate, and surface ligand, 1-dodecanethiol, were dissolved in a non-polar solvent, 1-octadecene, and heated to 80ºC. The reaction solution was then withdrawn in a glass syringe and loaded into a KD Scientific Legato microfluidic pump. The syringe was connected to PTFE tubing, with an inner diameter of 750 μm, and the reaction solution pumped through the controlled temperature zones before being collected in a glass vial for photoluminescence spectroscopy analysis. Specifications for the microfluidic reaction system are listed below in Table 2-1.
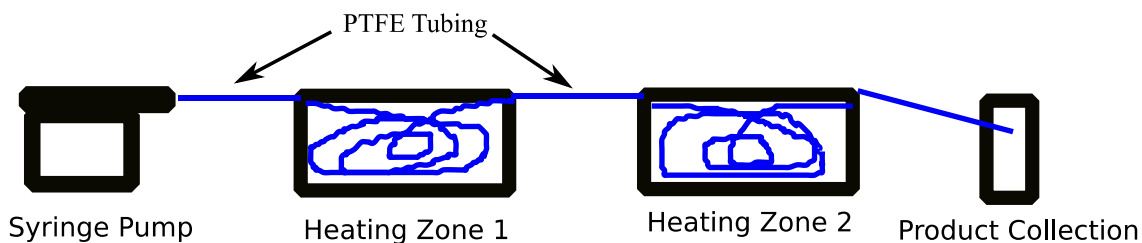
Figure 2-2: Microfluidic Reaction System.

Table 2-1: Microfluidic System Parameters

Flow Rate	0.01-1.0 mL/min
Superficial Velocity	2.2-220 cm/min
Heating Zone 1	200ºC
Heating Zone 2	180ºC
Residence Time (syringe pump to product collection)	0.5-45 min
Inner Diameter of PTFE Tubing	750 μm

QDSSC Assembly:

In this work CIS QDs were used as the primary absorbing layer for producing colloidal QDSSCs. A Colloidal Quantum Dot Sensitized Solar Cell architecture was used as described in the literature(Guijarro, Guillen et al. 2014, Kramer and Sargent 2014). A schematic of the cell design is shown in Figure 2-3.
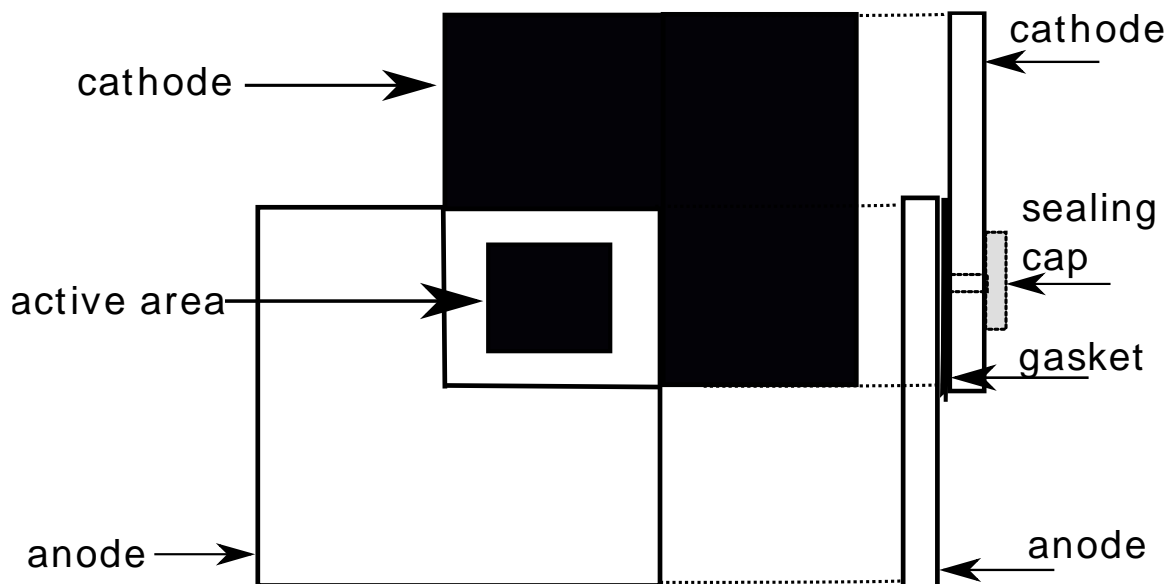
Figure 2-3: Experimental Solar Cell Schematic(Solaronix 2015).

Cell Fabrication:

The QD ligand, 1-dodecanethiol, acted as a molecular linker attaching the QDs to the titania electrodes after calcining for one hour at 500 °C. The pre fabricated titania anodes were placed in solutions of CIS QDs dispersed in dichloromethane, a procedure adapted from the literature (Yang, Kim et al. 2013, Guijarro, Guillen et al. 2014). After soaking overnight, the anodes were rinsed with ethanol and heated to 90°C on a hot plate. The gasket was then applied to the top of the anode and then the cathode was sealed on top of the gasket. The electrolyte solution was then injected with a vacuum syringe

through the pre-drilled hole. Finally, the hole was capped, forming a complete seal on the active area of the cell.

ZnS Passivating Layer:

In order to prevent the electrolyte from coming into direct contact with the QDs, which has shown to cause degradation, a passivating layer of zinc sulfide was applied on top of the QD absorbing layer (Guijarro, 2014). This technique is common among researchers producing QDSSCs, and uses a successive ionic layer absorption and reaction (SILAR) approach to deposit the zinc sulfide(Yang, Kim et al. 2013, Guijarro, Guillen et al. 2014). This procedure involved consecutively dipping the sensitized electrodes in aqueous solutions of 0.5 M zinc acetate and 0.5 M sodium sulfide, each for one minute, repeated twice.
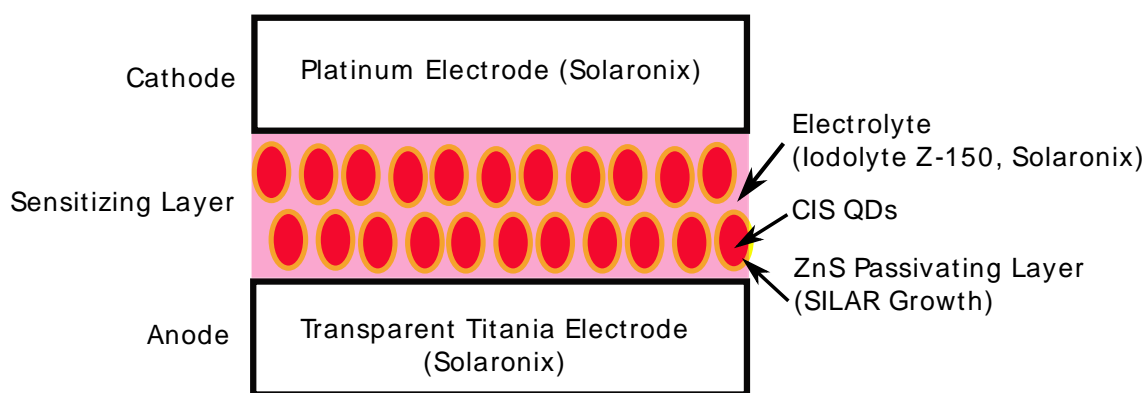
Figure 2-4: Experimental CIS QDSSC Design.

Characterization Methods:

Transmission electron microscopy (TEM) was performed to determine particle size for the QD samples. Images were analyzed with Image J to determine average QD size and standard deviation. TEM images were taken at an operating voltage of 100 kV using a Phillips CM10 TEM with Digital Camera Output.

Energy dispersive X-ray (EDX) spectroscopy was performed to compare the elemental composition of QD samples, using a Hitachi S-4500 field emission scanning electron

microscope with a Quartz PCI XOne SSD X-ray analyzer, at an operating voltage of 5 kV.

X-ray photoelectron spectroscopy (XPS) analyses were carried to determine surface chemistry of the QD samples, with a Kratos Axis Ultra spectrometer using a monochromatic Al K α source (15mA, 14kV). XPS can detect all elements except hydrogen and helium, probes the surface of the sample to a depth of 5-7 nm, and has detection limits ranging from 0.1 to 0.5 atomic percent depending on the element. The instrument work function was calibrated to give a binding energy (BE) of 83.96 eV for the Au 4f7/2 line for metallic gold and the spectrometer dispersion was adjusted to give a BE of 932.62 eV for the Cu 2p3/2 line of metallic copper. The Kratos charge neutralizer system was used on all specimens. Survey scan analyses were carried out with an analysis area of 300 x 700 microns and a pass energy of 160 eV. High resolution analyses were carried out with an analysis area of 300 x 700 microns and a pass energy of 20 eV. Spectra have been charge corrected to the main line of the carbon 1s spectrum (adventitious carbon) set to 284.8 eV. Spectra were analyzed using CasaXPS software (version 2.3.14).

A Nicolet 6700 fourier transform infrared (FTIR) spectrometer equipped with a smart ITR diamond horizontal attenuated total reflectance (ATR) accessory was used to collect absorbance spectra from 500-4000 cm^{-1} for confirming ligand functionalization on the QDs.

X-Ray diffraction (XRD) was used to confirm the crystal structure of the QD samples. Analysis was done using a Bruker D2 Phaser powder diffractometer using CuKα radiation (λ for Kα = 1.54059 Å) from 2θ = 0-100. Estimates for particle size were calculated based on equation (3-1), using the Diffrac.EVA XRD analysis software.

A Shimadzu UV-3600 UV-VIS-NIR spectrophotometer was used to collect the absorption spectrum of the QDs dispersed in toluene from 300-800nm.

A PTI photoluminescence spectrophotometer was used to measure the photoluminescence emissions of the QD samples. The QDs were dispersed in toluene and excited with an excitation wavelength of 400 nm. Emission spectra was collected from 420-800 nm.

Results and Discussion:

CIS QDs were first produced examining the HU and HI synthesis methods with different molar ratios of Cu:In. CIS QDs were also synthesized using a microfluidic technique with different flow rates, as seen below in Table 2-2. In order to determine the most effective synthesis method for making the CIS QDs, samples produced from these methods were compared using several characterization techniques. The most attractive feature of QDs is their ability to absorb and emit lights at different wavelengths. To characterize the optical performance of these QDs, UV-Visible and photoluminescence spectroscopies were used. These results are then further analyzed to determine QYs of the samples from different synthesis methods.

Photoluminescence spectroscopy was the first characterization technique performed on each QD sample as the emission spectrum profile is a quick way to determine the effectiveness of a synthesis method. Reaction solvent volumes from 5-50mL, most commonly 1-octadecene, were tested and it was found that for using 0.2 mmol of copper, and changing the amount of indium according to the desired molar ratio, in 10 mL of 1-octadecene, optimal QD products were produced. Synthesis procedures with three different molar ratios for HU and HI experiments were performed, with parameters listed in Table 2-2. Using equivalent sample concentrations, photoluminescence intensity counts in the range of 100 000s were achieved, an order of magnitude greater than QDs previously synthesized for similar applications(Allan 2012).

Table 2-2: Summary of HU and HI CIS QD Experiments

Sample Name	CIS-R1 (HU and HI)	CIS-R2 (HU and HI)	CIS-R3 (HU and HI)	CIS-R2 (Micro)	CIS-R2 (Micro)
Reaction Time (min)	60	60	60	2.7	0.6
Molar Ratio (Cu:In)	1:1	1:2	1:4	1:2	1:2

Transmission Electron Microscopy:

Transmission electron microscopy (TEM) was used to determine the average diameter and size distribution of the QDs. ImageJ software was used to determine size and standard deviation in each of the samples. Agglomeration of QDs synthesized from the hot-injection technique resulted in poor quality images of CIS QDs with molar ratio 1:1. TEM images from samples produced via HU and HI synthesis routes, and the corresponding data table can be seen below in Figure 2-5 and Table 2-3.
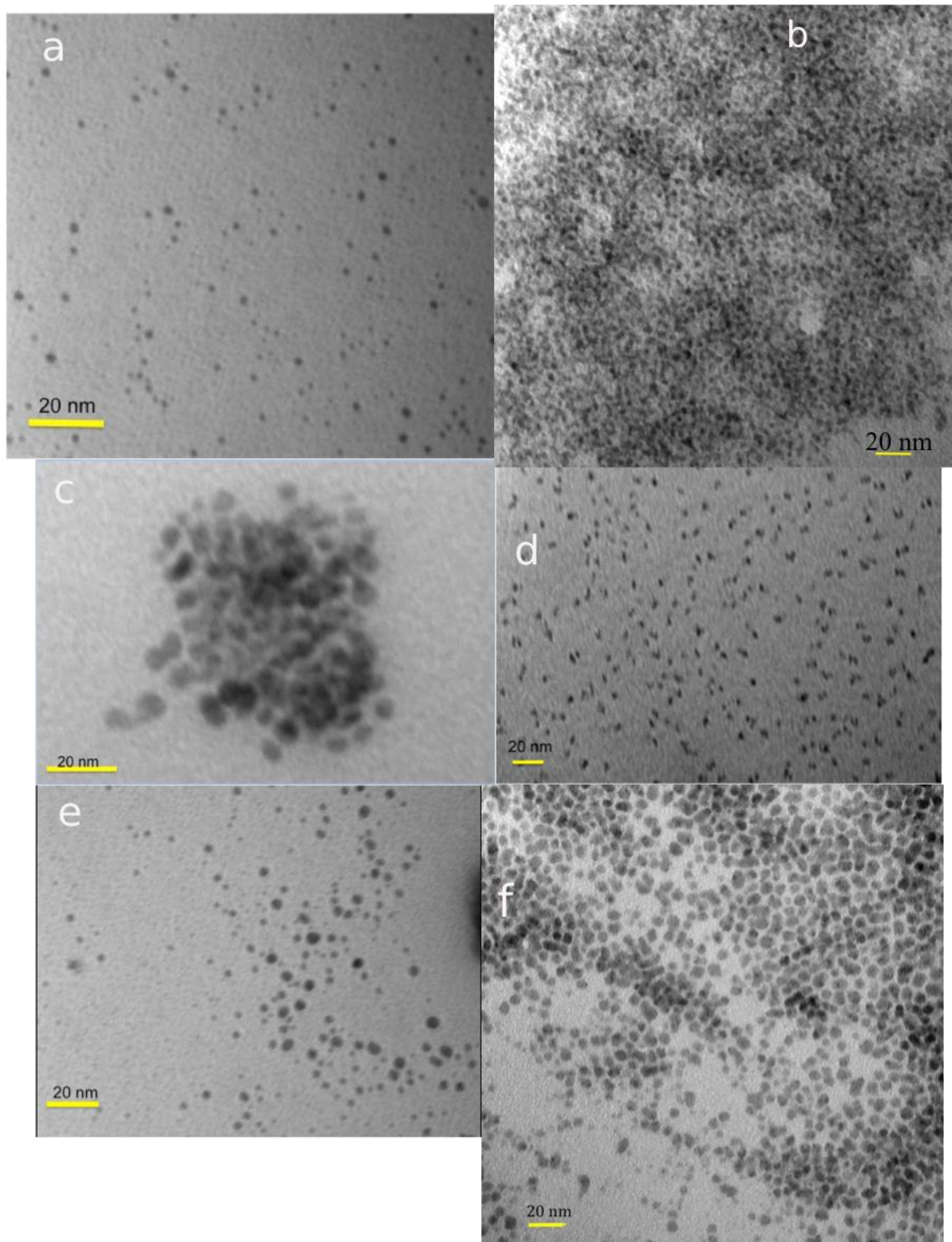
Figure 2-5: TEM images of CIS R1 HU (a), CIS R1 HI (b), CIS R2 HU (c), CIS R2 HI (d), CIS R3 HU (e), and CIS R3 HI (f).

Table 2-3: CIS QD Size Comparison

Sample	Average Diameter (nm)	Standard Deviation (nm)
Heat-Up:		
CIS R1	3.6	1.3
CIS R2	4.9	1.4
CIS R3	5.5	2.2
Hot-Injection:		
CIS R2	3.6	0.6
CIS R3	5.7	0.9
Literature Comparison:		
CIS (Yu, 2013)	3.4	0.4
CIS (Chang, 2013)	9.3	0.5
CIS (Song, 2012)	2.0-2.5	Widely dispersed

From these results it is clear that the heat-up technique produced a wider size distribution that also increased as the average QD size increased. This can be attributed to the QD growth occurring over a wider range of temperatures for the HU synthesis method. It can be seen that samples with increased indium content have a larger size in both synthesis methods. When comparing these results to those found in literature, a range of values have been reported (Song 2012, Chang 2013, Yu 2013) with the reported standard deviations being similar to those achieved by the HI method in this work (Song 2012, Chang 2013, Yu 2013). In most studies, either a HI or HU synthesis method is used, however results from this work show the difference between methods when keeping all other reaction variables constant.

TEM results for CIS R1 HI and CIS R2 Micro showed significant agglomeration, as seen below in Figures 2-6 and 2-7.

20 nm
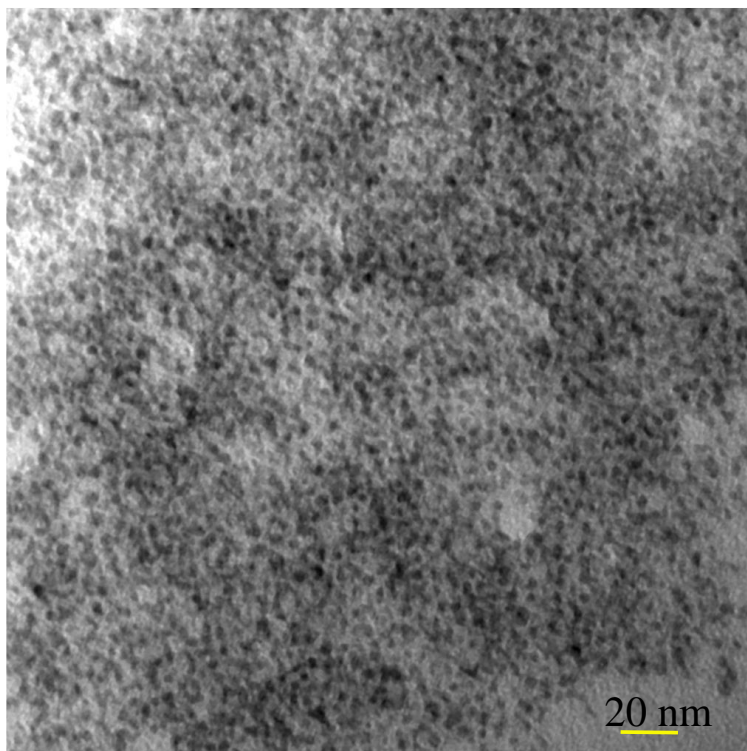
Figure 2-6: TEM image of CIS R1 HI.

20 nm
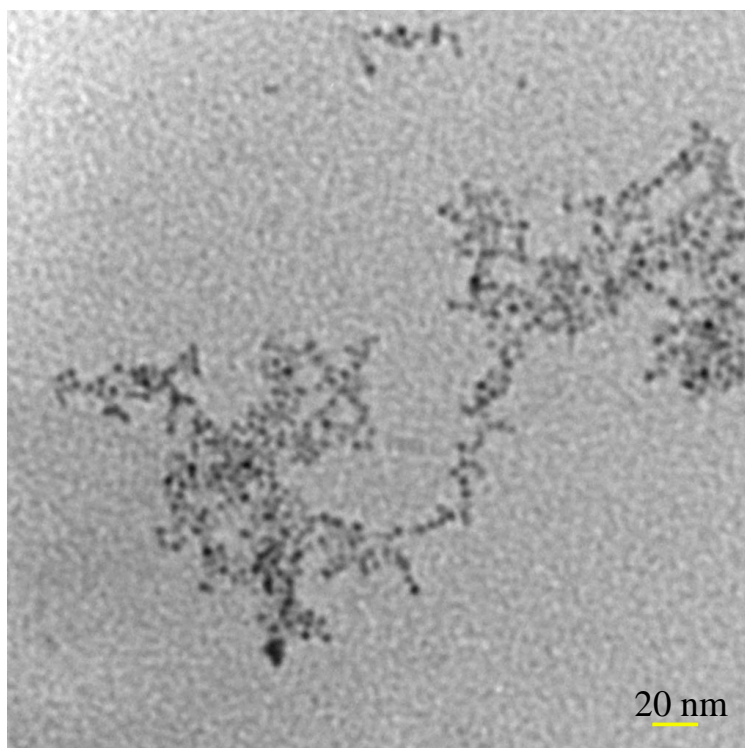
Figure 2-7: TEM image of CIS R2 Micro.

Energy-dispersive X-ray Spectroscopy:

EDX was used to determine the elemental composition of the QD samples produced from the HU and HI synthesis techniques.
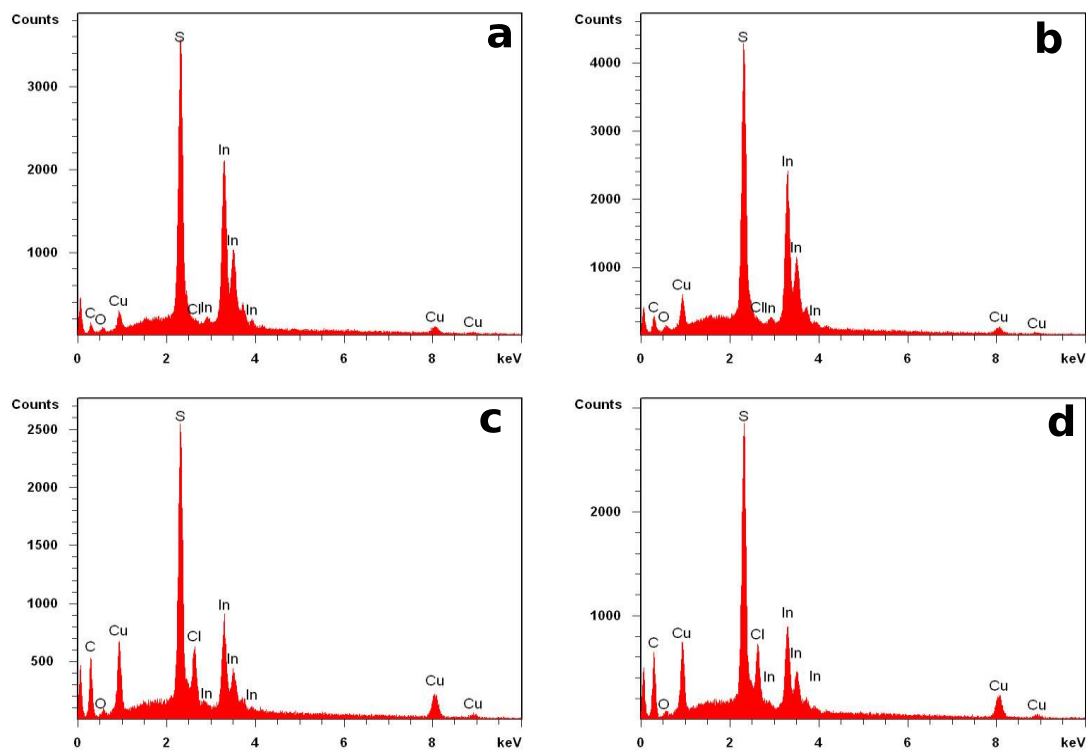
Figure 2-8: EDX Spectrum of CIS-R3-HI (a), CIS-R3-HU (b), CIS-R1-HI (c), and CIS-R1-HU (d).

Table 2-4: Summary of EDX Results for CIS-R1 HU/HI and CIS-R3 HU/HI

Element % Sample	C	O	S	Cu	In
R1-HU	44.7	1.2	16.4	18.0	15.0
R1-HI	42.8	1.1	16.7	19.4	15.6
R3-HU	22.3	4.3	25.1	6.8	40.9
R3-HI	14.6	2.2	27.0	8.6	46.9

When comparing samples produced from the two different methods it can be seen that the resulting compositions are very similar. During synthesis the molar ratio of Cu:In was 1:1

for R1 samples and 1:4 for R3 samples (Table 2-2). It can be seen that the carbon content, attributed to the QD ligand, is higher for the HU synthesis samples. This can be attributed to the ligand having more surface coverage on the QD, because of the longer time it is exposed to QDs during the crystal nucleation reaction. It can be seen that the amount of S present is dependent on the molar ratio of Cu:In. The S elemental percentage is consistent for both methods with each of the different molar ratios.

X-ray Photoelectron Spectroscopy:

Further to EDX, XPS was performed to determine specific chemical bonding of elements present within the QD samples. The survey spectrums of CIS R1 and CIS R2 from the HI method are compared below in Figure 2-9.
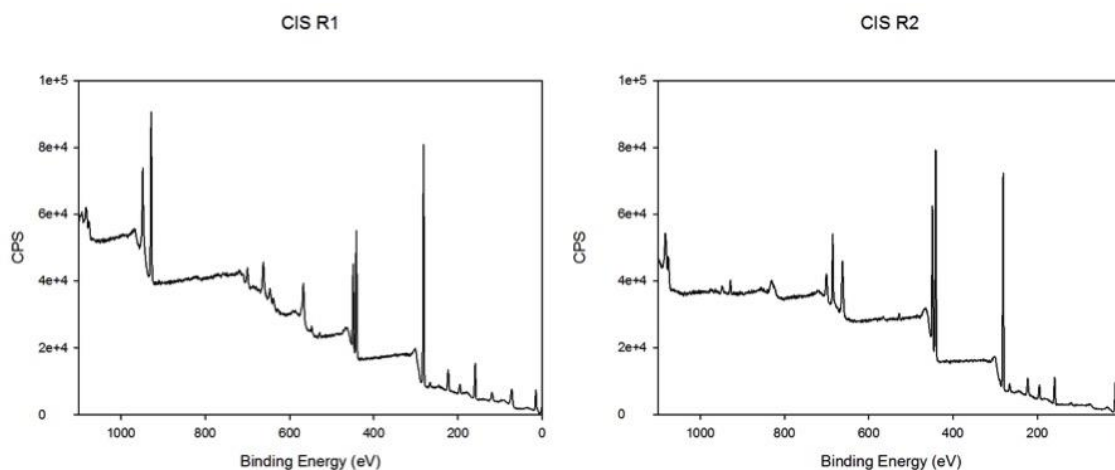
Figure 2-9: XPS Survey Spectrums of CIS R1 (left) and CIS R2 (right).

To characterize the CIS QDs, six characteristic peaks were examined, including indium 3d 5/2, indium 3d 5/2 - $M_4N_{45}N_{45}$ auger parameter, copper 2p 3/2, copper 2p 3/2 – $L_3M_{45}M_{45}$ auger parameter, carbon 1s, and sulfur 2p 3/2 and 1/2. The high resolution scans for each of these peaks can be seen below in Figure 2-10 and Figure 2-11 for CIS R1 and CIS R2, respectively.

CIS R1:
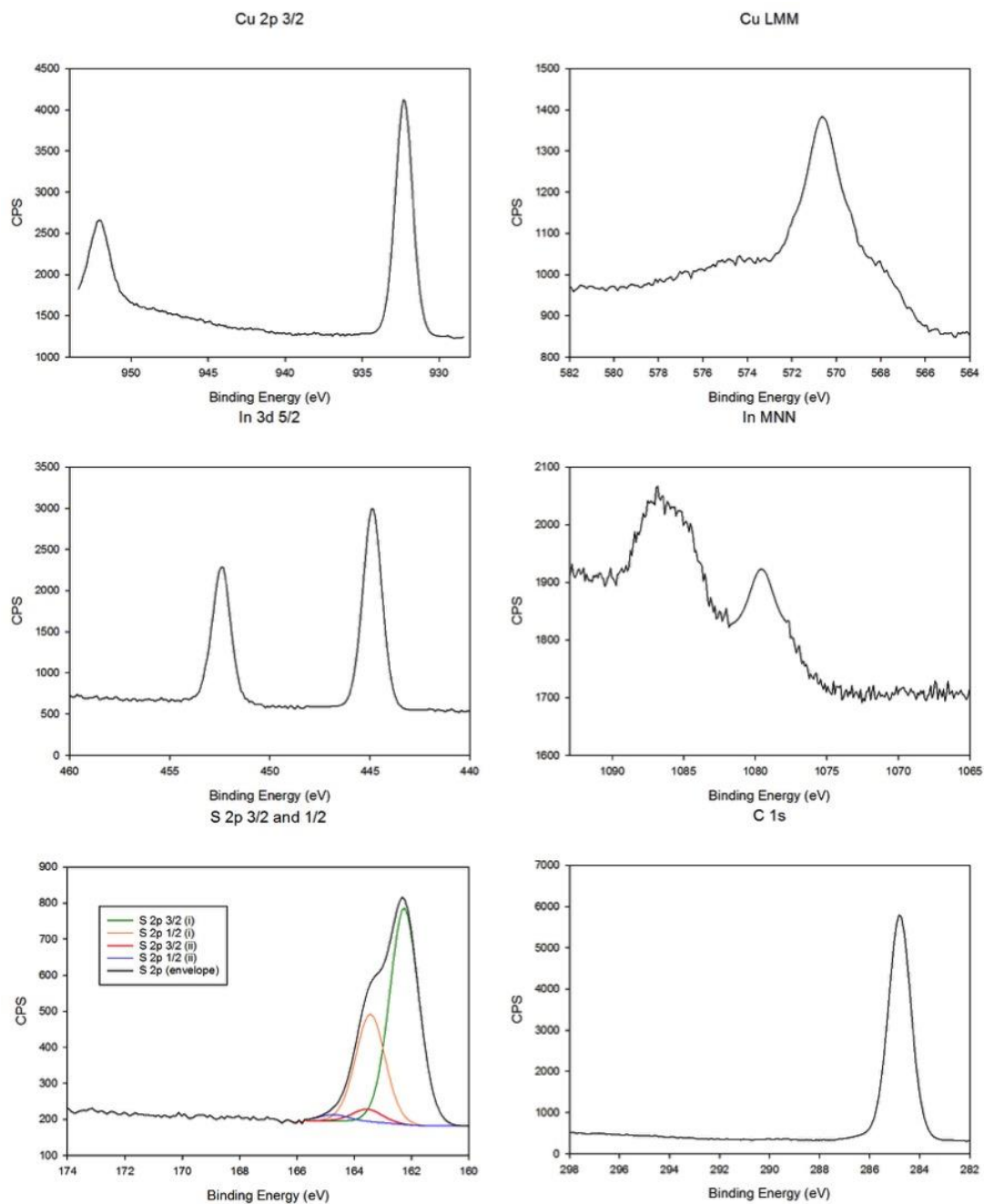
Figure 2-10: High Resolution XPS Scans for CIS R1 Peaks.

CIS R2
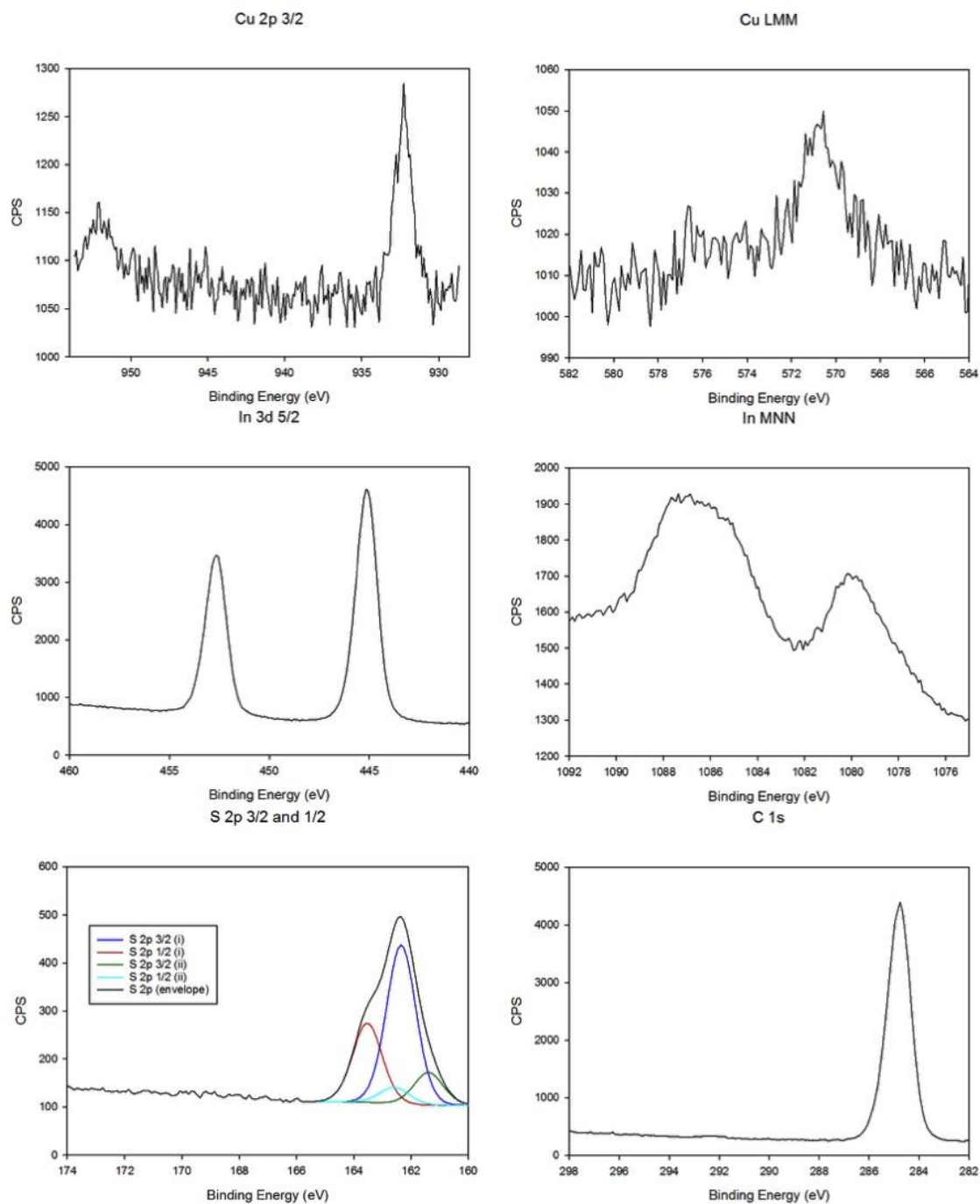
Figure 2-11: High Resolution XPS Scans for CIS R2 Peaks.

Table 2-5: XPS Peak Position Comparison

Peak	Peak Position (eV) (CIS R10		Peak Position (eV) (CIS R2)		Dominant Compound(Beamson 1992, Wagner 2003)
Cu 2p 3/2	932.29		932.31		**Cu(II) - CuS**
Cu LMM	570.63 Auger Parameter: 1848.4		570.76 Auger Parameter: 1848.3		**Cu(I) - CuS**
In 3d 5/2	444.88		445.14		**CuInS$_2$**
In MNN	1079.56 Auger Parameter: 852.03		1079.94 Auger Parameter: 851.9		**In$_2$S$_3$**
S 2p 3/2	162.26(i) (95%)	163.55(ii) (5%)	162.34(i) (83%)	161.39(ii) (17%)	**CuS, C-S-H (Thiol), CuInS$_2$**
S 2p 1/2	163.44(i)	164.73(ii)	163.52(i)	162.57(ii)	**Doublet separation from S 2p 3/2, +1.18 eV**
C 1s	284.80		284.80		**C-C, C-H (from QD ligand)**

Comparing the binding energies for each peak to those in the XPS database (Beamson 1992, Wagner 2003), the data in Table 2-5 confirms the chemical structure of the QD samples as being a mixture of CuInS$_2$, CuS, and In$_2$S$_3$. Analyzing the auger parameters as well for copper and indium allows for more insight into the dominant chemical species, as there is limited availability of XPS database data for specific binding energies from CuInS$_2$.The copper peaks indicate Cu(I) as being the dominant species in both samples. The indium auger parameter suggests In$_2$S$_3$ as being the dominant species, however the indium 3d 5/2 peaks correspond directly to the binding energy of CuInS$_2$, 444.9 +/- 0.4 eV (Wagner 2003). This suggests that there is a mixture of metal sulfides present in the samples, a commonly found result in literature (Lee, 2014). The C 1s peaks shows C-C and C-H as being the dominant species, which was expected from the ligand

functionalization on the QDs. These findings corroborate the previously discussed EDX results, showing that the QD samples produced have the structure of CIS_2.

Fourier Transform Infrared Spectroscopy:

As shown in Figure 2-12, peaks from approximately 1350-1450 and 2800-2900 are present from C-H bonds, characteristic of 1-dodecanthiol which is coated over the outer surface of the QDs, $CH_3(CH_2)_{10}CH_2SH$, indicating successful functionalization of the QDs with the surface ligand. These results are consistent with findings from EDX and XPS indicating ligand functionalization on the surface, resulting in C-H and C-C bonds.
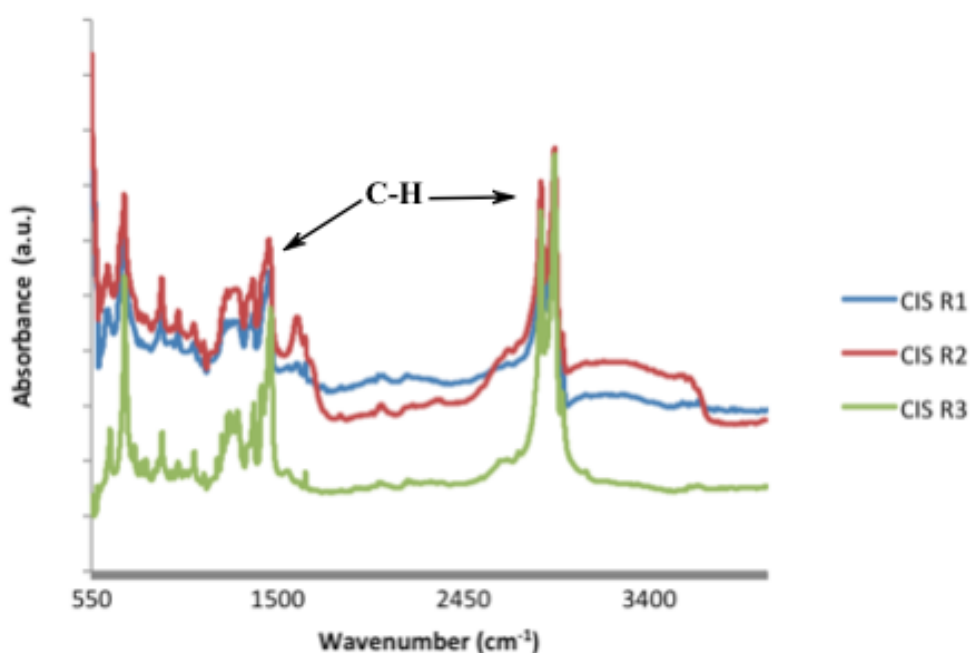
Figure 2-12: FTIR Absorbance Spectrum of CIS QDs.

X-ray Diffraction:

The XRD spectrum of CIS-R2-HU corresponds to bulk tetragonal chalcopyrite CIS, with characteristic peaks at 27, 47, and 55 degrees (Chang and Waclawik 2013). These results are consistent with EDX and XPS, indicating a CIS_2 tetragonal chalcopyrite crystal structure in the QD samples.
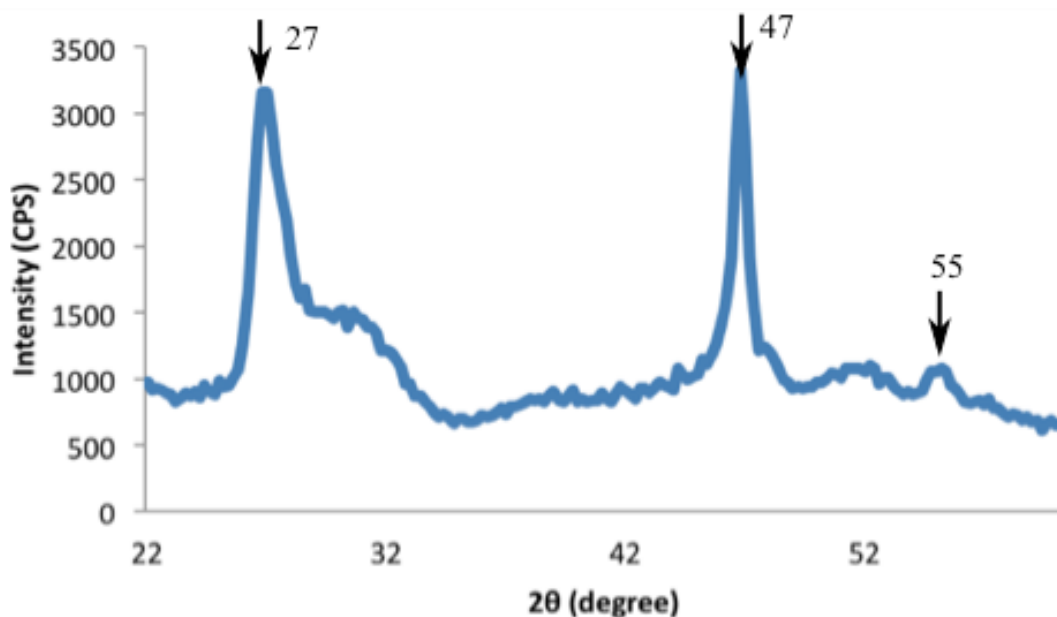
Figure 2-13: XRD Spectrum of CIS-R2-HU.

UV-Visible Spectroscopy and Photoluminescence Spectroscopy:

The absorbance profiles of CIS QDs produced by the investigated methods are very similar. Samples show strongest absorbance in the UV region, with some continuing into the visible range, making them ideal for applications requiring emission at 650 nm and higher. The only samples that actually produced visible absorption peaks were CIS-R2-HU and CIS-R2-HI, which can be seen in Figure 2-14.

Emission profiles for the different CIS QD samples were collected using an excitation wavelength of 400 nm for all samples, with strongest emissions from CIS-R2-HUand CIS-R2-HI shown in Figure 2-14, at 650 nm. For all samples an excitation wavelength of 400 nm was used, the excitation maximum was found by performing excitation scans with photoluminescence spectroscopy.
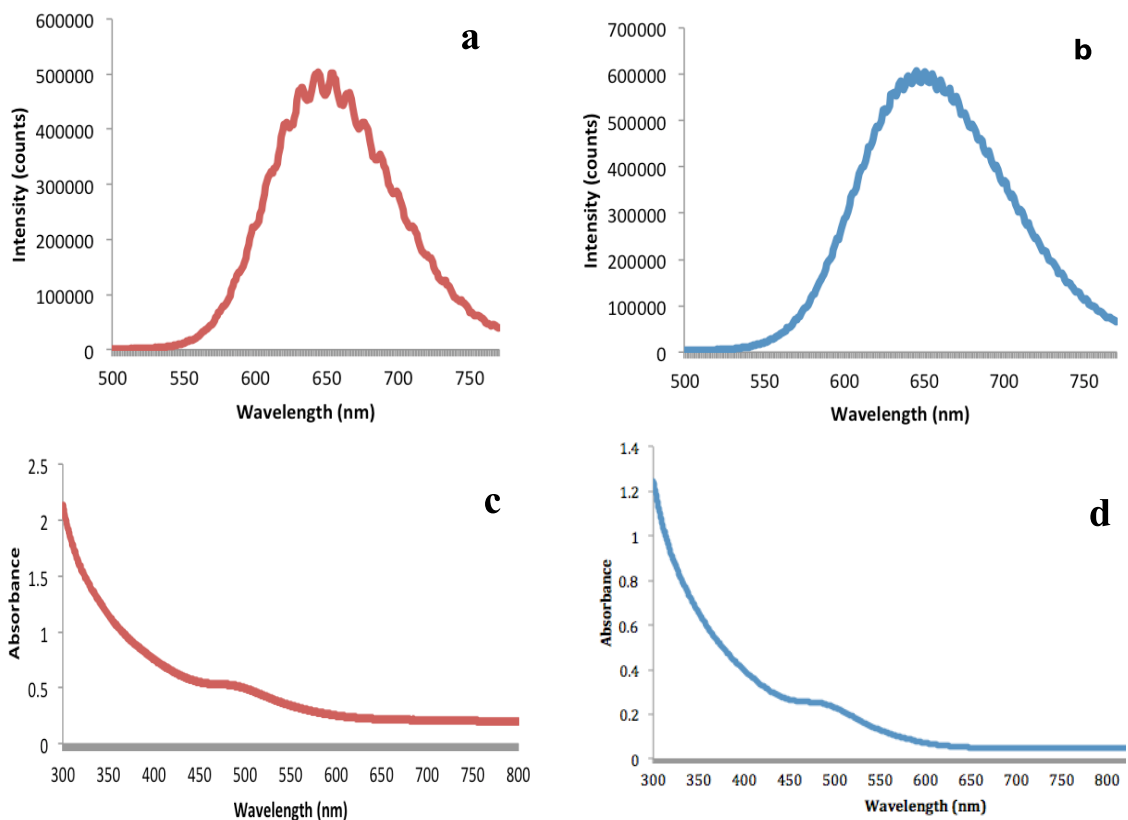
Figure 2-14: Absorbance and Emission Spectrums of CIS QDs. Emission Spectrum of CIS-R2-HU (a), Emission Spectrum of CIS-R2-HI (b), UV-Visible Absorbance Spectrum of CIS-R2-HU (c), and UV-Visible Absorbance Spectrum CIS –R2-HI (d).

It can be observed that the sample produced from the heat-up (HU) method has stronger absorbance, both at equal concentrations of CIS QDs. To perform QY calculations, the sample absorbance measurements were taken using UV-Visible Spectroscopy at very low concentrations to minimize light scattering, yielding absorbance values from 0.002-0.012 (Nanoco-Group-PLC 2013).

Samples produced from the microfluidic synthesis, with emission spectrum characteristic of CIS QDs at 650nm, showed very weak photoluminescence emissions, as seen in Figure 2-15. However one sample produced by the microfluidic synthesis, with a flow rate of 0.5 mL/min, resulted in a strong emission with the excitation wavelength at 350 nm, visible in Figure 2-16.
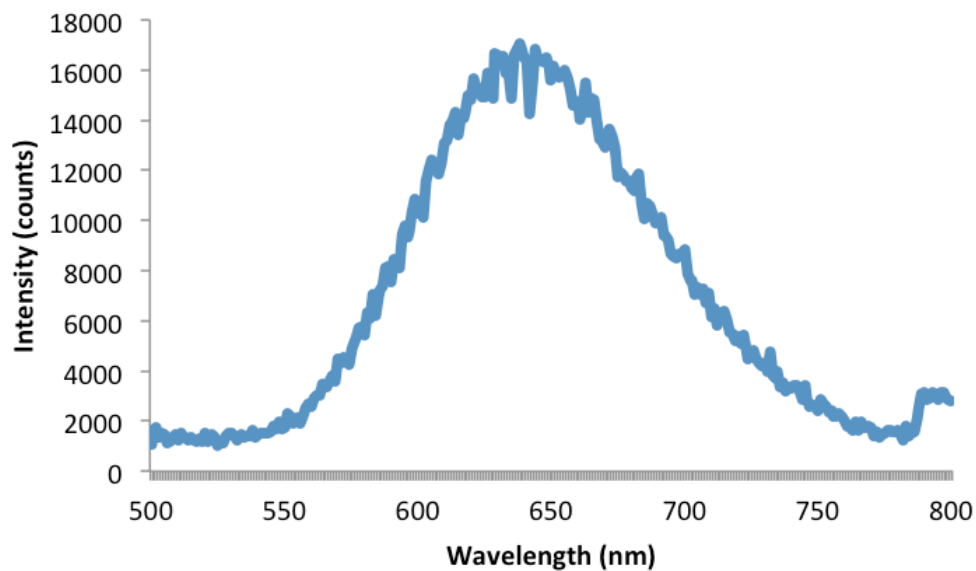
Figure 2-15: Emission Spectrum of CIS-R2-Micro with 0.1 mL/min flow rate.
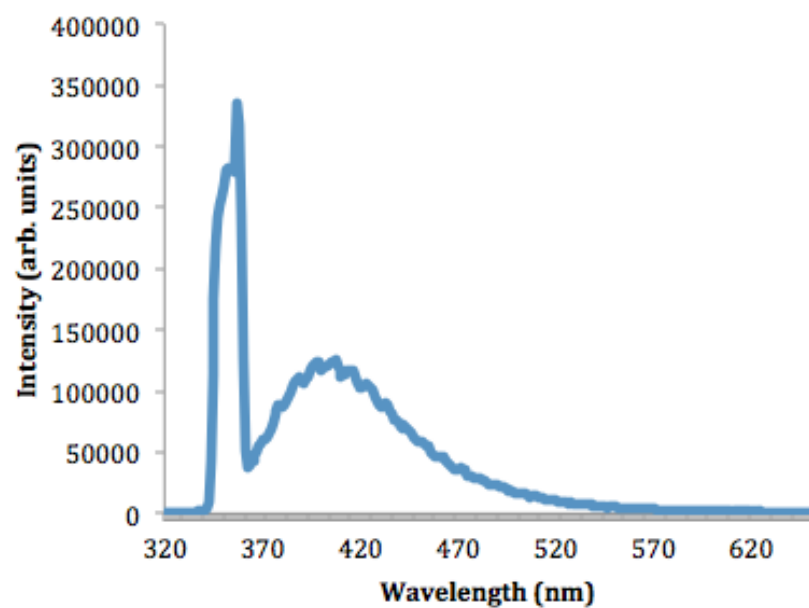
Figure 2-16: Emission Spectrum of CIS-R2-Micro with 0.5 mL/min flow rate.

Table 2-6: Comparison of Sample Photoluminescence Intensities

Sample	Peak Emission Intensity (counts)
CIS-R2-HU	500 000
CIS-R2-HI	600 000
CIS-R2-Micro with 0.1 mL/min flow rate	16 000

CIS-R2-Micro with 0.5 mL/min flow rate	130 000

When comparing the sample emission spectrums of the different methods it can be seen that the intensity is highest for the HI sample. Although it was expected that the different synthesis methods would produce different results, mostly due to different heat transfer rates and mixing conditions, the emission intensity is highly dependent on the concentration of QDs being tested. The QY can be used to normalize the effects of concentration and provide a comparison based on the absorption-emission efficiency of the QDs.

Quantum Yield:

The QY of a material is particularly important with light harvesting applications such as photovoltaics, with the QY defined as the ratio of photons absorbed to photons emitted. One of the main advantages of QDs is their ability to absorb light and convert it into more desirable wavelengths. The QY value is highly related to the performance of QDs in this area. The QY is greatly influenced by surface chemistry, such as trap sites in the QDs, ligands used, storage conditions and synthesis techniques. High QYs are characteristic to high-performance, higher quality QDs.

The QY was calculated using the following formula (Nanoco-Group-PLC 2013):

$$QY = QY_s \times \frac{A_x}{A_s} \times \frac{F_s}{F_x} \times \frac{N_x}{N_{s^2}}^2 \tag{2.1}$$

where A refers to the area under the photoluminescence emission spectrum, F refers to the absorbance value at the excitation wavelength, N refers to the refractive index of the solvent, s refers to the standard used, and x refers to the unknown sample.

In order to calculate the QY of the QDs produced in this work, first a suitable fluorescent dye was selected as the standard. The excitation wavelength used to excite the QDs must fall within the standard's excitation range. In the case of CIS QDs, which were excited using a wavelength of 400 nm, Coumarin 153 was selected as the reference

material based on an optimized QY procedure developed by Nanoco Inc.(Nanoco-Group-PLC 2013). Although the QY can be determined using one set of absorption and emission measurements from Coumarin 153, a more accurate, reproducible procedure involved constructing a calibration curve for the dye standard. Dye solutions containing Coumarin 153 dissolved in toluene of different concentrations were prepared and their absorbance was measured at 400 nm. Immediately after the absorbance measurements, photoluminescence measurements were carried out. This same procedure was used to develop the QD calibration curves also by dissolving QD powder in toluene at different concentrations. The area under the photoemission was then calculated, allowing a calibration curve relating absorbance to integrated photoluminescent area to be produced. Due to the high QY of most commercial dyes, dye solutions with absorbance values in the range of 0.002-0.012 were selected because more concentrated dye solutions produce substantial photoemissions, which lead to less accurate photoluminescence measurements(Nanoco-Group-PLC 2013).

Quantum Yield Calibration Curves
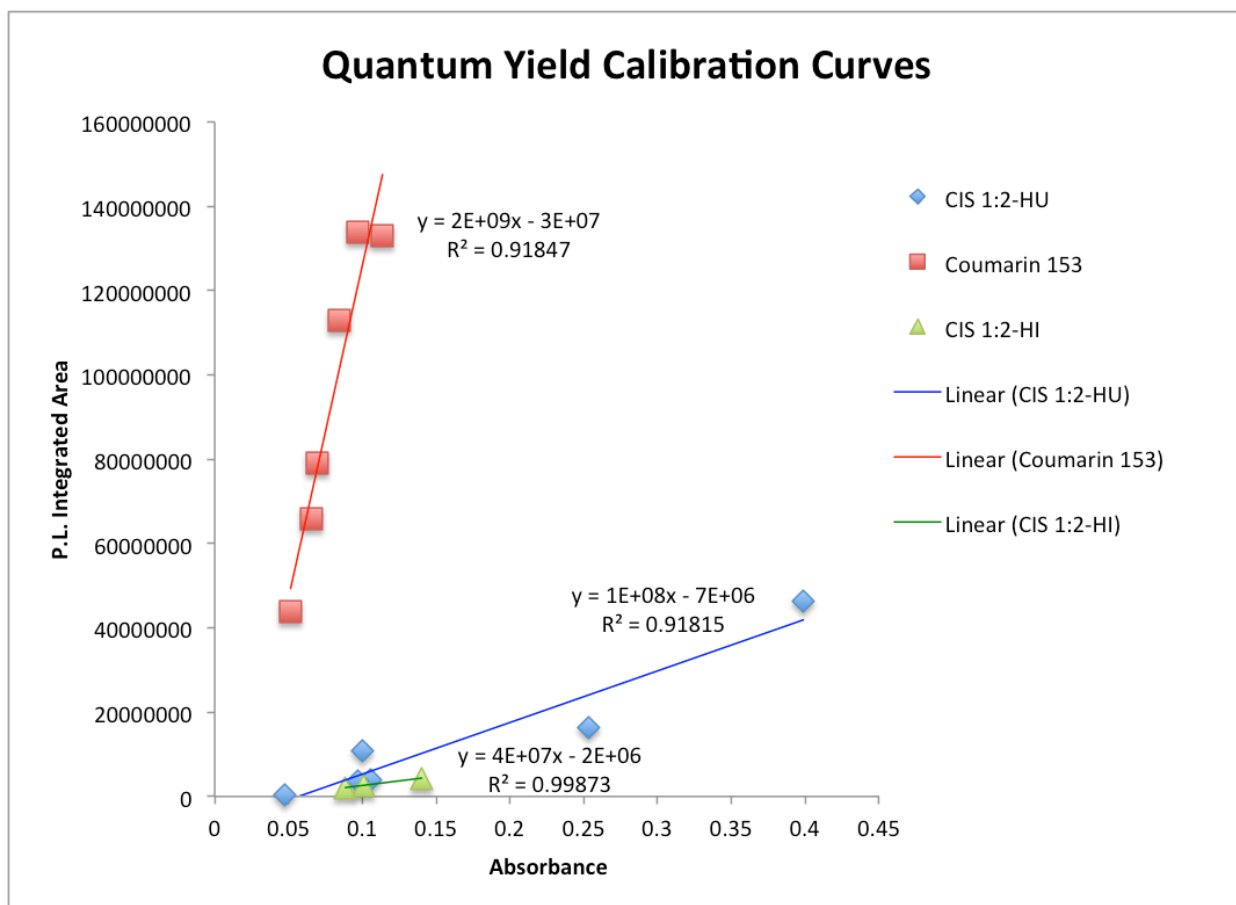
Figure 2-17: Experimental QY Calibration Curve for Coumarin 153, CIS-R2-HU, and CIS-R2-HI.

The linearized calibration curve can then be used to determine the QD's QY. The slope of the line was used to replace $\frac{F_s}{A_s}$ in the QY equation.

$$QY = QY_s \times \frac{A_x}{F_x} \times \frac{N_x^2}{N_{s^\wedge 2}} \times \frac{2}{10^9} \tag{2.2}$$

With this substituted equation, the QY can be determined for any QD sample that is excited in the range of 370-450 nm. For the CIS QDs produced in this work, several different concentrations of QD solutions were prepared and their absorbance and integrated photoemissions were plotted. The slopes of the linearized curves in Figure 2-6 were used to replace the value $\frac{A_x}{F_x}$ when determining the QY for those samples.

Table 2-7: QY of CIS QDs from different synthesis methods

Sample	Quantum Yield from Calibration Curves (%)
CIS R2 HU	7
CIS R2HI	2
CIS 1:2 Micro	6

From these results it is clear that the HU and microfluidic techniques produced the higher quality QDs. The photoluminescence intensity of the emission spectrum for CIS R2 HI was the highest, 600 000 counts, yet resulted in the lowest QY. These results indicate that the photoluminescence results, without considering QY, can be misleading and are highly dependent on the prepared sample concentration. Higher QYs were expected because results in literature using the HU technique have been shown to cause the ligand to bond to core atoms during crystal growth, opposed to surface bonding, which is more likely to occur in the HI technique(Chang and Waclawik 2013). This result is also interesting because even though the TEM results confirmed the HI route to produce a more narrow size distribution, it did not result in higher QY. The reason for lower QYs in this work compared to literature is likely due to delays between sample collection and analysis, and a lack of expertise in QD syntheses methods.

Quantum Dot Solar Cells:

A solar simulator was used to test the performance of the fabricated QDSSCs. Sample cells had an active area of 0.25 cm^2 and each cell was tested three times under 1 sun illumination (AM 1.5). Although the resulting efficiencies are much lower than those reported in literature, recent efficiencies in the range of 4-5% have been reported for QDSSCs using CIS QDs(Yang, Kim et al. 2013, Guijarro, Guillen et al. 2014), this is primarily due to lack of fabrication optimization. There is a small degree of error associated with the efficiency and fill factor values due to the instrument not being able to measure the voltage when the current drops below approximately 0.00001 A. This has a negligible effect on the resulting values.
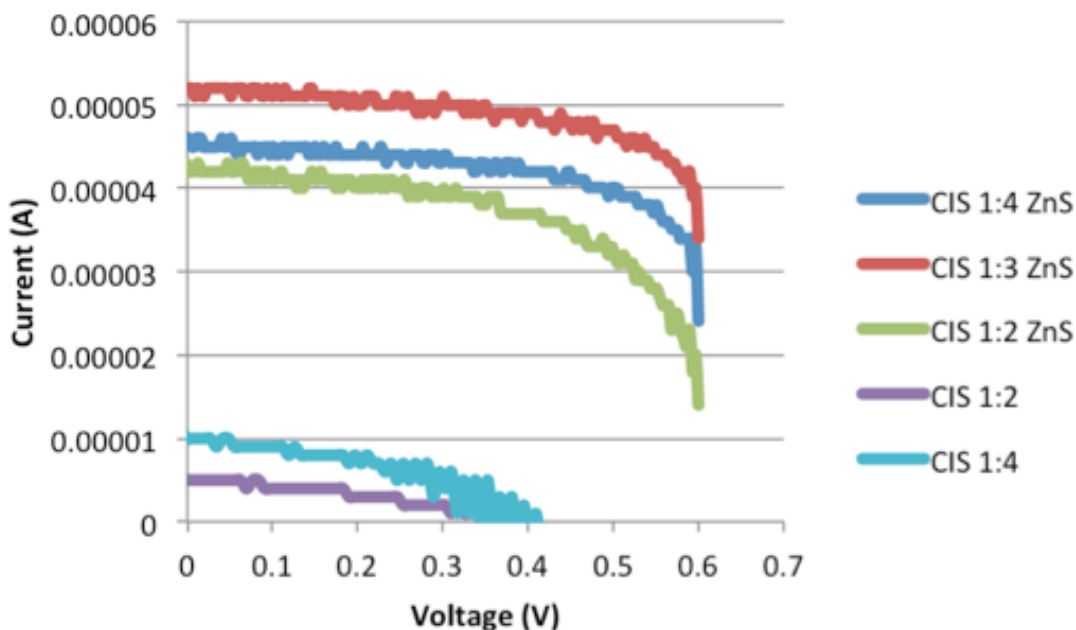
Figure 2-18: IV Curves for Experimental CIS QDSSCs.

Table 2-8: Summary of Experimental CIS QDSSC Performance

Sample	Efficiency (%)	Fill Factor (%)
CIS 1:2	0.003	36
CIS 1:4	0.008	50

CIS 1:2 with ZnS	0.07	60
CIS 1:3 with ZnS	0.1	78
CIS 1:4 with ZnS	0.08	71

From these results it can be seen that the addition of a ZnS layer from the SILAR method described in the experimental methods section, over the deposited QDs provides a magnitude increase in efficiency. This can be attributed to the additional layer preventing the electrolyte from degrading the QD absorbing layer. It can also be seen that the molar ratio of Cu:In plays an important role in the cell's performance. Samples with increased indium content have their absorption edge shifted to higher wavelengths, meaning they are capable of absorbing a wider range of sunlight. This was consistent with photoluminescence spectroscopy showing emission profiles of CIS QDs with higher indium content to be shifted to higher wavelengths. This results in an increase in efficiency and fill factor. The fill factor is a ratio between the maximum achievable power and the product of open circuit voltage and short circuit current. A higher fill factor indicates fewer internal losses. Recent studies on QDSSCs report fill factor values in the range of 50-70%, consistent with our results (Yang 2013, Guijarro 2014).

Conclusion:

This work characterized and compared the QD samples produced from three different synthesis techniques. Producing QDs with the desired light selective properties was confirmed by thoroughly analyzing their optical properties. QY was used to compare the quality of QDs produced from each method. TEM confirmed the size of QDs produced to be in the range of 3-6 nm.

It was found that the samples with molar ratio Cu:In 1:2 produced the most stable QDs with highest QY. It was also found that the HU synthesis method produced QDs with the highest QY, despite having a wider size distribution. Although many research efforts focus on reducing the size distribution, this can be a conflicting approach. It has

been shown that by introducing the sulfur-containing ligand prior to heating of the reaction solution, referred to in this work as the HU technique, the ligand molecule will bind to sulfur atoms both on the core and surface of the QD(Chang and Waclawik 2013). While the HI technique causes the ligand molecule to bind primarily to surface bound sulfur atoms on the QD(Chang and Waclawik 2013). EDX results confirm this by showing an increased carbon content for samples produced from the HU method. This leads to the conclusion that even though the HI technique has a more uniform growth temperature producing a narrow size distribution of products, it does not necessarily equate to higher quality QD products. Furthermore the difference in FWHM of the photoluminescence emission profiles for HU and HI techniques is not substantial.

In this work QDSSCs based on a liquid junction architecture were produced using CIS QDs. Samples with the highest resulting QY were used as the primary absorbing layer to fabricate QDSSCs. The effect of molar ratio and addition of a ZnS passivating layer was analyzed, showing that QDs with higher indium content result in higher efficiency. CIS QDs with higher indium content have a red shifted photoluminescence emission profile, meaning that they absorb a wider portion of the visible and near infrared spectrum, attributing to the increases seen in efficiency.

Results from this work shed new light on the differences between HU and HI CIS QD synthesis methods. The time at which the surfactant is added into the reaction solution was found to dramatically affect the optical and structural properties of the QD product. These properties were also shown to be significant when fabricating QDSSCs.

Bibliography

1. Allen, J. (2012). Light and Heat Selective Polymer Nanocomposite Films for Sustainable Greenhouses. M.E.Sc., The Univerisity of Western Ontario.
2. Beamson, G. and Briggs, D. High Resolution XPS of Organic Polymers - The Scienta ESCA300 Database Wiley Interscience, 1992.
3. Beard, M. C., J. M. Luther, O. E. Semonin and A. J. Nozik (2013). "Third generation photovoltaics based on multiple exciton generation in quantum confined semiconductors." AccChem Res 46(6): 1252-1260.
4. British-Petroleum (2014). BP Energy Outlook 2035. London England.

5.   Chang, J. and E. R. Waclawik (2013). "Controlled synthesis of CuInS2, Cu2SnS3 and Cu2ZnSnS4 nano-structures: insight into the universal phase-selectivity mechanism." CrystEngComm 15(28): 5612.

6.   Choi, S. H., E. G. Kim and T. Hyeon (2006). "One-pot synthesis of copper-indium sulfide nanocrystalheterostructures with acorn, bottle, and larva shapes." J Am ChemSoc 128(8): 2520-2521.

7.   Connor, S. (2011). Solution Processing for Copper Indium Sulfide Solar Cells. Doctorate, Stanford University.

8.   Group, W. R. (2012). "Lead-salt Semiconductor Quantum Dots." 2015, from http://wise.research.engineering.cornell.edu/index.html.

9.   Guijarro, N., E. Guillen, T. Lana-Villarreal and R. Gomez (2014). "Quantum dot-sensitized solar cells based on directly adsorbed zinc copper indium sulfide colloids." PhysChemChemPhys 16(19): 9115-9122.

10.   H. Zhang, K. C. (2012). "Efficient CdSe quantum dot-sensitized solar cells prepared by a postsynthesis assembly approach." Chemical Communication 48: 11235-11237.

11.   Han, W., L. Yi, N. Zhao, A. Tang, M. Gao and Z. Tang (2008). "Synthesis and shape-tailoring of copper sulfide/indium sulfide-based nanocrystals." J Am ChemSoc 130(39): 13152-13161.

12.   Hines, D. A. and P. V. Kamat (2014). "Recent advances in quantum dot surface chemistry." ACS Appl Mater Interfaces 6(5): 3041-3057.

13.   Jensen, K., Marre, S., Baek J., Park, J., and Bawendi, M. Journal of Laboratory Automation, December 2009; vol. 14, 6: pp. 367-373.

14.   Kamat, P. (2014). "Solar Cell Research." from http://www3.nd.edu/~kamatlab/research_solarCells.html.

15.   Kamat, P. V. (2013). "Quantum Dot Solar Cells.The Next Big Thingin Photovoltaics." The Journal of Physical Chemistry Letters 4(6): 908-918.

16.   Katsuhiro Nose, T. O., and Shinya Otsuka-Yao-Matsuo (2008). "Colloidal Synthesis of Ternary Copper Indium Diselenide Quantum Dots and Their OpticalProperties." Journal of Physical Chemistry 113: 3455-3460.

17.   Kongkanand, A., K. Tvrdy, K. Takechi, M. Kuno and P. V. Kamat (2008). "Quantum dot solar cells. Tuning photoresponse through size and shape control of CdSe-TiO2 architecture." J Am ChemSoc 130(12): 4007-4015.

18.   Kramer, I. J. and E. H. Sargent (2014). "The architecture of colloidal quantum dot solar cells: materials to devices." Chem Rev 114(1): 863-882.

19.   Lan, X., J. Bai, S. Masala, S. M. Thon, Y. Ren, I. J. Kramer, S. Hoogland, A. Simchi, G. I. Koleilat, D. Paz-Soldan, Z. Ning, A. J. Labelle, J. Y. Kim, G. Jabbour and E. H. Sargent (2013). "Self-assembled, nanowire network electrodes for depleted bulk heterojunction solar cells." Adv Mater 25(12): 1769-1773.

20.   Lee, J., & Han, C.-S. (2014). Large-scale synthesis of highly emissive and photostable CuInS2/ZnS nanocrystals through hybrid flow reactor. Nanoscale Research Letters, 9(1), 78. 1556

21.   Lee, S. H., H. Jin, D. Y. Kim, K. Song, S. H. Oh, S. Kim, E. F. Schubert and J. K. Kim (2014). "Enhanced power conversion efficiency of quantum dot sensitized solar cells with near single-crystalline TiO(2) nanohelixes used as photoanodes." Opt Express 22 Suppl 3: A867-879.

22. Lee, S. S., K. W. Seo, J. P. Park, S. K. Kim and I. W. Shim (2007). "Deposition of CuInS2 thin films using copper- and indium/sulfide-containing precursors through a two-stage MOCVD method." InorgChem 46(3): 1013-1017.

23. Li, L., A. Pandey, D. J. Werder, B. P. Khanal, J. M. Pietryga and V. I. Klimov (2011). "Efficient synthesis of highly luminescent copper indium sulfide-based core/shell nanocrystals with surprisingly long-lived emission." J Am ChemSoc 133(5): 1176-1179.

24. Li, M., W. Ni, B. Kan, X. Wan, L. Zhang, Q. Zhang, G. Long, Y. Zuo and Y. Chen (2013). "Graphene quantum dots as the hole transport layer material for high-performance organic solar cells." PhysChemChemPhys 15(43): 18973-18978.

25. Li, T.-L., Y.-L. Lee and H. Teng (2012). "High-performance quantum dot-sensitized solar cells based on sensitization with CuInS2quantum dots/CdSheterostructure." Energy Environ. Sci. 5(1): 5315-5324.

26. Ma, W., S. L. Swisher, T. Ewers, J. Engel, V. E. Ferry, H. A. Atwater and A. P. Alivisatos (2011). "Photovoltaic performance of ultrasmallPbSe quantum dots." ACS Nano 5(10): 8140-8147.

27. Maraghechi, P., A. J. Labelle, A. R. Kirmani, X. Lan, M. M. Adachi, S. M. Thon, S. Hoogland, A. Lee, Z. Ning, A. Fischer, A. Amassian and E. H. Sargent (2013). "The donor-supply electrode enhances performance in colloidal quantum dot solar cells." ACS Nano 7(7): 6111-6116.

28. McDaniel, H., N. Fuke, N. S. Makarov, J. M. Pietryga and V. I. Klimov (2013). "An integrated approach to realizing high-performance liquid-junction quantum dot sensitized solar cells." Nat Commun 4: 2887.

29. McDaniel, H., N. Fuke, J. M. Pietryga and V. I. Klimov (2013). "Engineered CuInSexS2–xQuantum Dots for Sensitized Solar Cells." The Journal of Physical Chemistry Letters 4(3): 355-361.

30. Mesolight. (2014). "Quantum Dot Products." from http://www.mesolight.com

31. Mora-Sero, I., S. Gimenez, F. Fabregat-Santiago, R. Gomez, Q. Shen, T. Toyoda and J. Bisquert (2009). "Recombination in quantum dot sensitized solar cells." AccChem Res 42(11): 1848-1857.

32. Nanoco-Group-PLC (2013). Methods for the determination of photoluminescence quantum yield

33. Nanoco-Group-PLC. (2014). "Quantum Dots manufactured in Bulk Quantities." 2014, from http://www.nanocotechnologies.com/index.aspx.

34. Nanotech, O. (2014). "Products Catalogue ", from http://www.oceannanotech.com/catalog.php.

35. Ning, Z., D. Zhitomirsky, V. Adinolfi, B. Sutherland, J. Xu, O. Voznyy, P. Maraghechi, X. Lan, S. Hoogland, Y. Ren and E. H. Sargent (2013). "Graded doping for enhanced colloidal quantum dot photovoltaics." Adv Mater 25(12): 1719-1723.

36. NREL. (2012). "Novel Physical Principles Research Thrust." 2015, from http://www.centerforadvancedsolarphotophysics.org/physical_principles.html.

37. NREL. (2014). "National Center for Photovoltaics." 2015, from http://www.nrel.gov/ncpv/.

38. Pan, Z., I. Mora-Sero, Q. Shen, H. Zhang, Y. Li, K. Zhao, J. Wang, X. Zhong and J. Bisquert (2014). "High-efficiency "green" quantum dot solar cells." J Am ChemSoc 136(25): 9203-9210.

39. PB Kreider, K. K., CH Chang (2014). "Two-step continuous-flow synthesis of CuInSe 2 nanoparticles in a solar microreactor." RSC Advances 4(27): 13827-13830.

40. Queisser, W. S. a. H. J. (1961). "Detailed Balance Limit of Efficiency of p- n Junction Solar Cells." Journal of Applied Physics 32: 510-519.

41. Rath, A. K., M. Bernechea, L. Martinez and G. Konstantatos (2011). "Solution-processed heterojunction solar cells based on p-type PbS quantum dots and n-type Bi2 S3 nanocrystals." Adv Mater 23(32): 3712-3717.

42. Semonin, O. E., J. M. Luther and M. C. Beard (2012). "Quantum dots for next-generation photovoltaics." Materials Today 15(11): 508-515.

43. Shen, F., W. Que, Y. Liao and X. Yin (2011). "Photocatalytic Activity of TiO2Nanoparticles Sensitized by CuInS2Quantum Dots." Industrial & Engineering Chemistry Research 50(15): 9131-9137.

44. Sigma-Aldrich. (2014). "Quantum Dots - Products." from http://www.sigmaaldrich.com/materials-science/material-science-products.html?TablePage=16376883.

45. Sigma-Aldrich. (2015). "Quantum Dots." from http://www.sigmaaldrich.com/materials-science/nanomaterials/quantum-dots.html.

46. Solaronix. (2015). "Test Cell Spare Parts." from http://shop.solaronix.com.

47. Song, W.-S. and H. Yang (2012). "Efficient White-Light-Emitting Diodes Fabricated from Highly Fluorescent Copper Indium Sulfide Core/Shell Quantum Dots." Chemistry of Materials 24(10): 1961-1967.

48. Stolle, C. J., T. B. Harvey and B. A. Korgel (2013). "Nanocrystal photovoltaics: a review of recent progress." Current Opinion in Chemical Engineering 2(2): 160-167.

49. Sungwoo Kim, M. K., Seajin Kim, Jin-HyukHeo, Jun Hong Noh, Sang HyukIm, Sang IlSeok, and Sang-Wook Kim (2013). "Fabrication of CuInTe2 and CuInTe2xSex Ternary Gradient Quantum Dots and Their Application to Solar Cells." ACS Nano.

50. Wagner, C.D., Naumkin, A.V., Kraut-Vass, A., Allison, J.W., Powell, C.J., Rumble, J. NIST Standard Reference Database 20, Version 3.4 (web version) (http:/srdata.nist.gov/xps/) 2003.

51. Yang, J., J. Y. Kim, J. H. Yu, T. Y. Ahn, H. Lee, T. S. Choi, Y. W. Kim, J. Joo, M. J. Ko and T. Hyeon (2013). "Copper-indium-selenide quantum dot-sensitized solar cells." PhysChemChemPhys 15(47): 20517-20525.

52. Yu, K., P. Ng, J. Ouyang, M. B. Zaman, A. Abulrob, T. N. Baral, D. Fatehi, Z. J. Jakubek, D. Kingston, X. Wu, X. Liu, C. Hebert, D. M. Leek and D. M. Whitfield (2013). "Low-temperature approach to highly emissive copper indium sulfide colloidal nanocrystals and their bioimaging applications." ACS Appl Mater Interfaces 5(8): 2870-2880.

CHAPTER 3: NANOCOMPOSITE THIN-FILMS FOR DOWN-CONVERSION APPLICATION

Abstract:

The top layer of silicon photovoltaic cells consists of a protective polymer, most commonly poly(ethyleneco-vinyl-acetate) (EVA), which is used to prevent degradation of the cell's performance by protecting it from environmental elements such as moisture and excessive heat. Potentially, QDs can be used to modify the incoming spectrum of sunlight before it is absorbed by silicon in these devices, converting light previously wasted, mostly in the form of thermalization losses, into the optimal wavelength of light for silicon to absorb, a process referred to as down-conversion.

In this work, QDs were melt mixed with EVA 1075 at 120 °C for 10 minutes using a twin screw mini extruder and pressed into thin films, 100 μm and 250 μm thickness. Resulting thin films were analyzed using UV-Visible spectroscopy and evaluated for their potential to provide efficiency increases when applied to silicon solar cells. QD-EVA thin films reduced average UV transmission to as low as 25% and showed potential to provide efficiency increases from 0.6-3 %.

Introduction:

The most current research discoveries are enabling scientists to produce solar cells with efficiencies in the range of 30-50 %, a massive improvement over the current standard in the North American photovoltaic industry of 15-18% for first generation cells (NREL 2014). However these new high-performance cells are still very expensive to produce, with most current manufacturers using conventional silicon devices which provide the highest watt output/cost(Kamat 2013, Kramer and Sargent 2014). Another hindrance with new generation solar cells is that their manufacturing process is very different from first generation cells, making it less desirable for current photovoltaic manufacturers to change their technology(Kamat 2013). A new approach that can help increase output at a very low cost is applying down-conversion technology to first generation cells, which also can be extended into emerging solar cell designs. Down-conversion is a process involving the conversion of a single high-energy photon into multiple lower-energy photons. This phenomenon is especially desirable for applications requiring the conversion of high-energy UV light into visible and near infrared light. With an optimal design this process has the potential to provide efficiency increases up to 5.5%(Yao Zhu 2013, NREL 2014). Down-conversion can also be applied in greenhouses to reduce plant-damaging UV light transmission, and convert it to visible light promoting photosynthesis.

Polymer-nanocomposites are an emerging class of materials with exceptional properties. Although nanomaterials have excellent performance features for many applications they are easily degraded by oxidation. Polymers are being used to stabilize

nanomaterials by providing a matrix for the nanomaterials and protecting them from oxygen degradation. In this work poly(ethylene-co-vinyl acetate)(EVA), a commonly used polymer for protecting photovoltaic cells, and copper indium sulfide CIS QDs were used to produce transparent nanocomposite films. Specifically EVA 1075, vinyl acetate content approximately 10%, was selected as the polymer for making QD-polymer films, which was previously investigated for down-conversion applications utilizing cadmium sulfide QDs (Xu 2009, Allan 2012, Allan et al. 2014). The resulting nanocomposite films from this work have two main potential areas of application. First as a down-conversion layer for boosting the efficiency of first generation solar cells and second as a UV blocking layer for greenhouses.

For both applications the main function of the nanocomposite thin film is to modify the incoming spectrum of light. The goal for both applications makes it desirable to convert as much UV light, 200-400nm, as possible into lower energy, higher wavelength light. For solar cell applications, the nanocomposite thin film would be applied at the end of the manufacturing process as the top-laminating layer. This would allow the sun's incoming light spectrum to be better matched to the absorbance spectrum of the primary absorbing layer in the solar cell, such as crystalline silicon for first generation solar cells. The exact thickness of the silicon-absorbing layer being used would dictate the required emission wavelength from the down-conversion layer(W.G.J.H.M. van Sark 2012).

In the case of down-conversion for greenhouse application, it is essential to selectively block ultraviolet light which causes damage to the plants. By applying a nanocomposite thin film as the greenhouse film, the amount of useful light, visible and near infrared, reaching the plants can be increased. This will lead to increased productivity for the greenhouse by promoting photosynthesis in the plants.

Down-Conversion for Solar Cells:

In North America the amount of solar energy contacting the earth, commonly referred to as "insolation", is approximately 1000 W/m^2. First generation silicon solar

cells are able to utilize only 468 W/m^2 of this energy, yielding efficiencies from 15-18% (Yao Zhu 2013, NREL 2014). This means we can expect to generate approximately 150-180 W/m^2 of active solar panel area. Researchers have shown down-conversion has the potential to exploit an additional 149 W/m^2 (Yao Zhu 2013). By utilizing all of the energy available for down-conversion, the fraction absorbed by silicon would increase to 617 W/m^2, raising the overall efficiency by as much as 5.5%.

An efficiency increase of 5.5% would require the down-conversion layer to absorb 100% of the available down-conversion fraction, without interrupting the current fraction utilized by silicon. It would also require perfect alignment between the band gap of silicon and emission wavelength of the down-converting layer. Although these conditions are difficult to achieve, efficiency gains in the range of 2-3% are feasible.

In 2007 a study was performed by Chung et al. with Eu^{3+} ions with an emission wavelength 600 nm, embedded in EVA as a down-conversion layer for crystalline silicon solar cells (Chung 2007). A relative increase in efficiency of 2.9% was observed. An efficiency increase of 1.2% was recorded in 2004 by Svrcek et al. when using silicon nanocrystals as a down converting layer (Svrcek V 2004). There have been other reports on other down-conversion materials, with efficiency increases in the range of 1-5% (W.G.J.H.M. van Sark 2012).

CIS QDs were chosen for this application for their tunable emission wavelength range and capability for QYs higher than 70%. By utilizing different synthesis conditions, CIS QDs can be modified to emit light from the visible region to near infrared region, approximately 550-950 nm, optimal for band gap alignment with a variety of silicon based solar cells. The band gap for multicrystalline silicon is 1.12 eV and 1.77 eV for amorphous silicon. Silicon cells with thinner absorbing layers can have a band gap up to 2.25 eV. The optimal wavelength of monochromatic light for a single-junction solar cell is equal to: wavelength $= \frac{1240}{E_g}$, where the wavelength is in nm and band gap (Eg) in eV (W.G.J.H.M. van Sark 2012). Using this equation, the optimal down converted emission wavelengths for silicon based solar cells are from 550 nm for thin films to 1100 nm for multicrystalline silicon.

Down-Conversion for Greenhouses:

A down-conversion layer for greenhouses provides simultaneous absorption of plant-damaging UV light and an increase in photosynthesis-driving light. The function of the QD-EVA thin film in a greenhouse application is similar to the down-conversion application for solar cells, with the main difference being the emission wavelength. Instead of matching the emission wavelength to the band gap of the absorbing material, the emission wavelength for a greenhouse is selected based on the plants' optimal absorption wavelengths for promoting photosynthesis. Chlorophyll and carotenoids are the pigments in plants primarily responsible for absorbing light essential for photosynthesis (Baker 2012). Most of the absorption occurs between 420 and 520 nm, with chlorophyll peaks also appearing from 650-675 nm. Although the emission profile of CIS QDs cannot be tuned below 530 nm, they would still be able to convert harmful UV light into emissions centered around 650-675 nm. Zinc oxide is a commonly used absorber of UV light and has characteristic emission tunable from approximately 400-600 nm, making it a better candidate for use in greenhouse down-conversion.

Quantum Dot Emission Spectrum Modification:

A typical emission spectrum for CIS QDs ranges from 650-950 nm(Song and Yang 2012, Yu, Ng et al. 2013). The emission wavelength requirement for down-conversion in first generation solar cells ranges from 550-1100 nm. The optimal emission wavelengths for down-conversion in greenhouses are from 430-530 nm and 650-675 nm(Baker 2012). This makes it necessary to evaluate techniques capable of blue shifting the emission spectrum of the CIS QDs. Zinc oxide is a well-known and effective UV absorber. Zinc oxide nanoparticles have been used as a down-conversion layer (Yao Zhu 2013) and zinc sulfide is commonly used as a shell layer over the QD core to improve photoluminescent intensity and increase the optical band gap (Guijarro, Guillen et al. 2014). In an effort to shift the emission wavelength of the CIS QDs to lower wavelengths, they were alloyed with different molar ratios of zinc. The effect of molar ratio and reaction time were compared for four different reactions using the HU synthesis method.

Experimental Section:

Quantum Dot Synthesis:

Materials:

Copper (II) chloride ($CuCl_2$, 99.995%, Sigma Aldrich), indium (III) acetate ($In(C_2H_3O_2)_3$, 99.99%, Sigma Aldrich), zinc acetate ($(CH_3CO_2)_2Zn$, 99.99%, Sigma Aldrich), 1-dodecanethiol ($CH_3(CH_2)_{11}SH$, 98%, Sigma Aldrich), and 1-octadecene ($CH_3(CH_2)_{15}CH=CH_2$, 90%, Sigma Aldrich) were used without further purification. Anhydrous methanol (99.8%) and toluene (99.9%, CHROMASOLV Plus) were purchased from Sigma Aldrich and used as received. CIS QDs (from HI and HU synthesis), Zinc oxide nanopowder (ZnO, 97%, Sigma Aldrich), and Poly(ethylene-co-vinyl acetate) 1075 (10% vinyl acetate, Sigma Aldrich) were used without further purification.

Methods:

In this work CIS QDs were synthesized using hot-injection (HI) and heat-up (HU) hydrothermal methods. In a typical HU synthesis, 0.2 mmol of copper (copper (II) acetate), 0.4 mmol of indium (indium (III) acetate), 2.0 mL of 1-dodecanethiol, and 8.0 mL of octadecene were combined in a 50 mL three-neck reaction flask. The reaction solution was then heated to 80 °C under vacuum for 30 minutes. It was then rapidly heated to 200 °C, where it was maintained for 60 minutes before collecting the QD products. The HI synthesis followed the same procedure except for the 2.0 mL of 1-dodecanethiol being injected into the reaction flask once the reaction solution reached 200 °C. CIS QDs alloyed with zinc were synthesized using the HU method. In a typical synthesis, 0.1-0.4 mmol of zinc, 0.2 mmol of copper, 0.2-0.4 mmol of indium, 2.0 mL of 1-dodecanethiol, and 8.0 mL of octadecene were combined in a 50 mL three-neck reaction flask. The reaction solution was then heated to 80 °C under vacuum for 30 minutes. It was then rapidly heated to 200 °C and samples were recovered after 10, 30, and 60 minutes of reaction time.

The samples were allowed to cool to room temperature, with a subsequent addition of a non-polar solvent such as chloroform or toluene to help disperse the QD particles, followed by addition of a polar solvent, methanol to precipitate the QD particles. The suspension was centrifuged at 6000 rpm for 10 minutes, with the supernatant being discarded and the QD precipitate being dispersed in toluene, followed by addition of methanol before centrifuging again at 6000 rpm for 10 minutes. This washing process was repeated at least twice to ensure the final product is free of unreacted precursors. The QD powder was then dried overnight in a vacuum oven at 80 ^{0}C.

$$(CH_3CO_2)_3Zn + CuCl2 + In(C_2H_3O2)_3 \xrightarrow[\text{DDT + ODE}]{200\ ^oC} \overset{\text{Quantum Dots}}{Zn_2CuIn2}$$
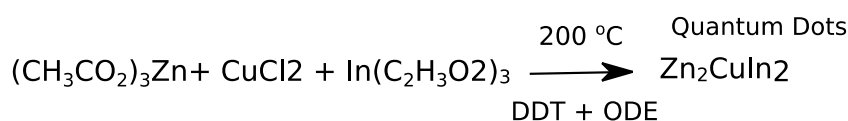
Figure 3-1: Reaction schematic of forming ZCIS QDs from zinc acetate, copper (II) chloride, and indium (III) acetate.

Nanocomposite Thin-Film Fabrication:

Methods:

CISQDs used for this application were selected based on their absorbance profiles and QYs. QDs synthesized with molar ratio Cu:In, 1:2 from both HI and HU methods were processed with EVA to produce nanocomposite thin films.

The melt mixing of CIS QDs with EVA 1075 was performed using a twin-screw mini extruder (Thermo-Electron, thermo scientific haake model: minilab II). In a typical procedure, approximately 2 g of EVA 1075 was loaded in to the extruder and allowed to mix for 5 min at 130 °C. Then the QDs were loaded, (4 mg for 0.1 wt%, 8 mg for 0.2 wt%, and 20 mg for 0.5 wt%) into the extruder with an additional 2 g of EVA 1075. The extruder was then allowed to mix for 10 min before collection of the QD-EVA extrudant. To press the extrudant into thin films a Universal film maker (Thermo Universal film maker S/N: 0016-010) and carver hydraulic press were used. First the appropriate amount of extrudant was weighed out and loaded into the film maker, 0.030 g for 100 μm films and 0.065 g for 250 μm films. The films were then pressed at 2500 psi, at 120 °C for 10 minutes, followed by product cooling before they were collected for analysis. To provide

a better idea on the UV absorbance strength of the CIS-EVA films, films produced with commercial ZnO nanopowder (particles with diameter less than 50 nm), a well-known UV absorber, were also prepared and compared to CIS-EVA films. Each thin-film was prepared with two repeats and UV-Visible transmission measurements were carried out three times for each film, with negligible differences arising.

Characterization Methods:

Energy dispersive X-ray (EDX) spectroscopy was performed to compare the elemental composition of QD samples using a Hitachi S-4500 field emission scanning electron microscope with a Quartz PCI XOne SSD X-ray analyzer, at an operating voltage of 5 kV.

X-ray photoelectron spectroscopy (XPS) analyses were carried to determine surface chemistry of the QD samples, with a Kratos Axis Ultra spectrometer using a monochromatic Al K α source (15mA, 14kV). XPS can detect all elements except hydrogen and helium, probes the surface of the sample to a depth of 5-7 nm, and has detection limits ranging from 0.1 to 0.5 atomic percent depending on the element. The instrument work function was calibrated to give a binding energy (BE) of 83.96 eV for the Au 4f7/2 line for metallic gold and the spectrometer dispersion was adjusted to give a BE of 932.62 eV for the Cu 2p3/2 line of metallic copper. The Kratos charge neutralizer system was used on all specimens. Survey scan analyses were carried out with an analysis area of 300 x 700 microns and a pass energy of 160 eV. High resolution analyses were carried out with an analysis area of 300 x 700 microns and a pass energy of 20 eV. Spectra have been charge corrected to the main line of the carbon 1s spectrum (adventitious carbon) set to 284.8 eV. Spectra were analysed using CasaXPS software (version 2.3.14).

X-Ray diffraction (XRD) was used to confirm the crystal structure of the QD samples. Analysis was done using a Bruker D2 Phaser powder diffractometer using CuKα radiation (λ for Kα = 1.54059 Å) from 2θ = 0-100. Estimates for particle size were calculated based on equation (3-1), using the Diffrac.EVA XRD analysis software.

A Shimadzu UV-3600 UV-VIS-NIR spectrophotometer with integrating sphere attachment was used to collect the transmission spectrum of the QD-EVA thin films from 200-800nm.

A PTI photoluminescence spectrophotometer was used to measure the photoluminescent emissions of the QD samples. The QDs were dispersed in toluene and excited with an excitation wavelength of 400 nm. Emission spectra was collected from 420-800 nm.

Results and Discussion:

In this work CIS QDs synthesized from HU and HI synthesis methods were analyzed for their use in thin films. The effect of alloying CIS QDs with zinc was examined by synthesizing ZCIS QDs using a HU synthesis method. The effect of different Zn:Cu:In molar ratios and reaction times were investigated as shown in Table 3-1. First the QDs were analyzed with Energy-dispersive X-ray Spectroscopy, X-ray Photoelectron Spectroscopy, and X-ray Diffraction to determine the elemental structure. The luminescent properties of the QDs were then analyzed with Photoluminescence Spectroscopy. The main features of the nanocomposite films analyzed in this study were their light-selective properties and long-term stability. To characterize the transmission of light through the films UV-Visible Spectroscopy was used. The emission profile of light from the films can be characterized using Photoluminescence Spectroscopy. However, combining the fact that light emission from solid samples is much more difficult to detect than in liquid samples and the relatively low QY of QDs produced in this work, significant emission spectrums from the films were not able to be collected. Scanning electron microscopy was used to compare the surface morphology of QD-EVA thin films with different QD loading percentages.

Quantum Dot Samples:

Table 3-1: Summary of CIS and ZCIS QD Experiments

Sample Name	Reaction Time (min)	Molar Ratio (Cu:In)
CIS-R1-HU	60	1:2
CIS-R1-HI	60	1:2

ZCIS HU:		Molar Ratio (Zn:Cu:In)
ZCIS-R1	10-60	1:2:2
ZCIS-R2	10-60	1:1:1
ZCIS-R3	10-60	2:1:1
ZCIS-R4	10-60	2:1:2

*All reactions were carried out at 200 ºC with 1-octadecene as the reaction solvent.

Energy-dispersive X-ray Spectroscopy:

The elemental compositions of QD samples produced from different reactions, and different reaction times for reaction R4, were compared as shown in Figure 3-2. Carbon present in the samples is from the QDs' ligand, 1-dodecanethiol, which was found to be inversely proportional to the amount of copper and indium present in the QDs. It has been shown in the literature that copper and indium make up most of the QD's core, with zinc creating a shell layer around the core (Semonin, Luther et al. 2012, Song and Yang 2012, Guijarro, Guillen et al. 2014). It can therefore be assumed that samples with reduced copper and indium content have a smaller core size and subsequently smaller overall diameter. This would equate to an overall higher content of ligands present in the QD samples, resulting in a higher elemental percentage of carbon. The chlorine is present from the copper chloride precursor, despite multiple washing steps with the QD products. Aluminum present was added to the samples during analysis to improve their conductivity.
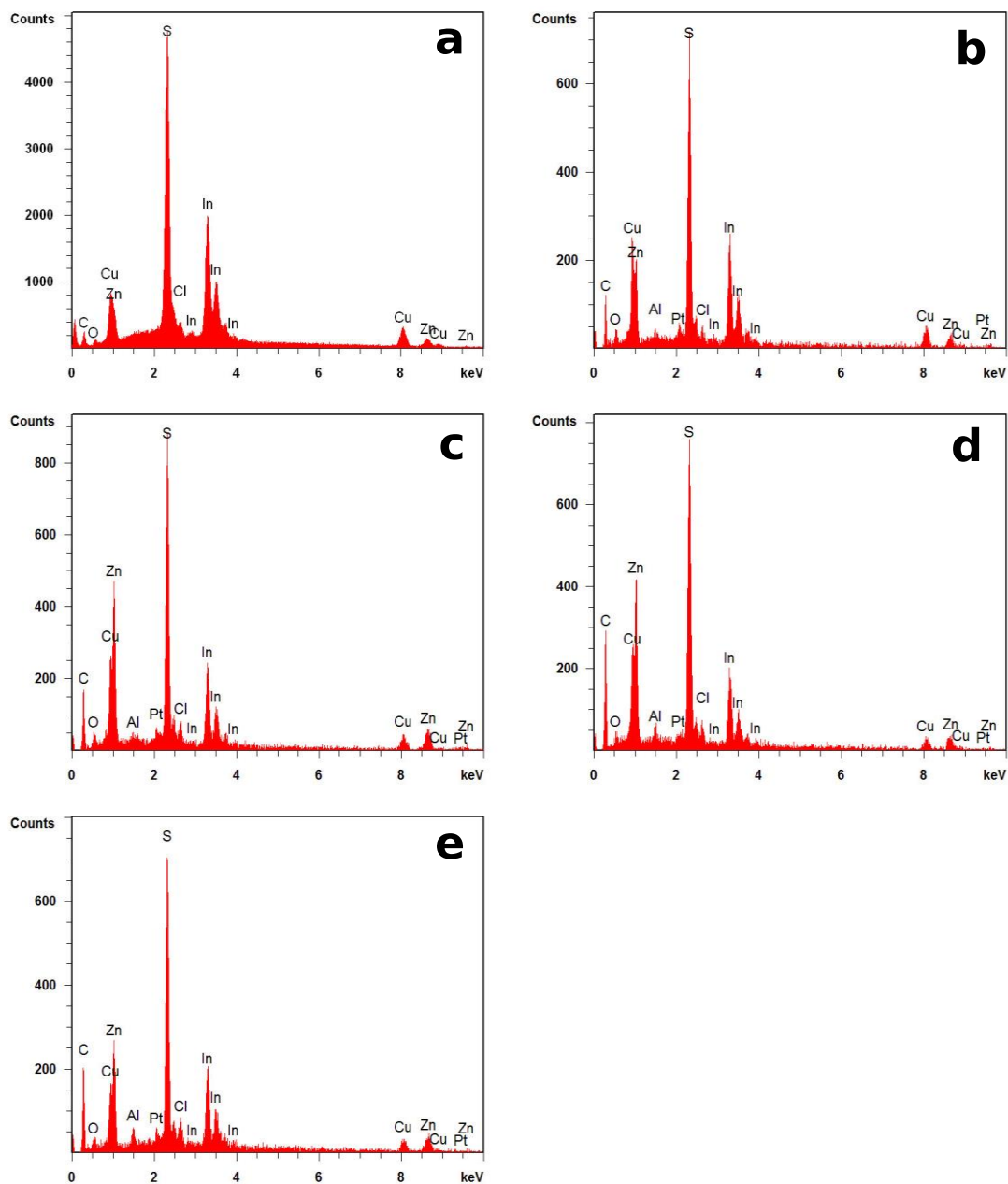
Figure 3-2: EDX Spectrum of ZCIS R1 60 minute reaction (a), ZCIS R2 60 minute reaction (b), ZCIS R3 60 minute reaction (c), ZCIS R4 60 minute reaction (d), and ZCIS R4-10 minute reaction (e).

Table 3-2: Summary of ZCIS EDX Results

Element % Sample	C	O	Al	S	Cl	Zn	Cu	In
R1-60 min	17.3	0.8	/	23.8	1.4	11.3	17.6	26.7
R2-60 min	23.7	4.1	0.4	17.3	1.0	16.4	17.9	19.3
R3-60 min	27.7	3.1	0.3	16.8	1.3	24.2	12.4	14.1
R4-10 min	37.3	2.4	0.5	16.1	1.8	17.7	10.3	14.0
R4-60 min	43.0	3.2	0.4	15.0	1.2	16.6	9.2	12.0

From Table 3-3 it can be observed that the molar ratio of Zn:Cu is fairly consistent between the precursor solution and the final products. However the amount of indium present in the product is significantly less than what was initially in the precursor solution. This can be attributed to a combination of the indium precursor being less reactive than the other two precursors and the dominant crystal structure of ZCIS QDs having a limit on the amount of indium present in the lattice, as confirmed by XRD analysis (below).

Table 3-3: Molar ratio comparison between precursor solution and final products

Sample	Precursor Molar Ratio (Zn:Cu:In)	Product Molar Ratio (Zn:Cu:In)
R1-60 min	1 : 2 : 2	0.6 : 1 : 0.9
R2-60 min	1 : 1 : 1	0.9 : 1 : 0.6
R3-60 min	2 : 1 : 1	1 : 0.5 : 0.3
R4-10 min	2 : 1 : 2	1 : 0.6 : 0.5
R4-60 min	2 : 1 : 2	1 : 0.6 : 0.4

X-ray Photoelectron Spectroscopy:

XPS was performed to determine the specific chemical bonding of elements present within the QD samples. The survey spectrum of ZCIS R1 can be seen below in Figure 3-3.
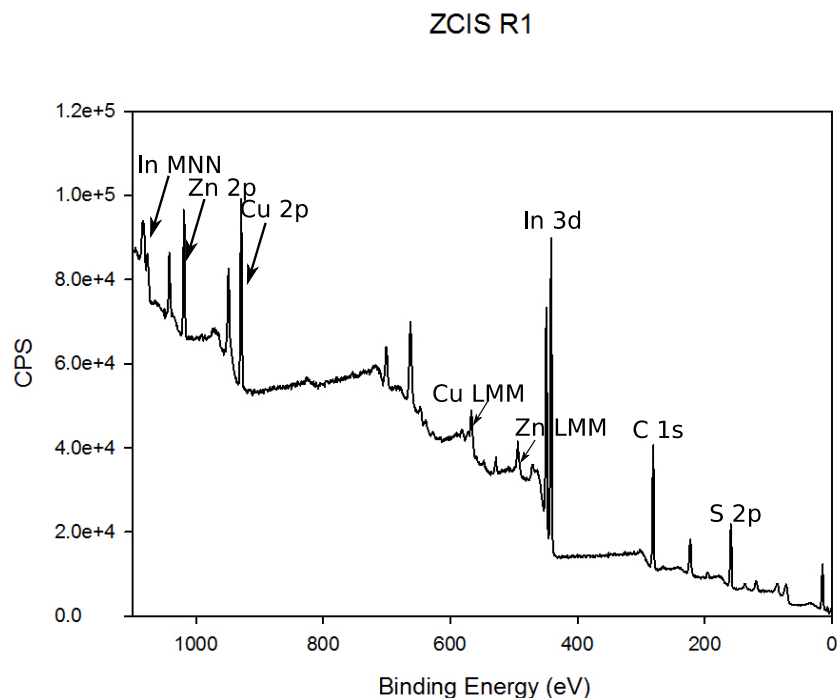
ZCIS R1

Figure 3-3:XPS Survey Spectrum of ZCIS R1.

To characterize the ZCIS QD sample, eight characteristic peaks were examined, including, zinc 2p 3/2, zinc 2p 3/2 - $L_3M_{45}M_{45}$ auger parameter, indium 3d 5/2, indium 3d 5/2 - $M_4N_{45}N_{45}$ auger parameter, copper 2p 3/2, copper 2p 3/2 – $L_3M_{45}M_{45}$ auger parameter, carbon 1s, and sulfur 2p 3/2 and 1/2. The high resolution scans for each of these peaks can be seen below in Figure 3-4.
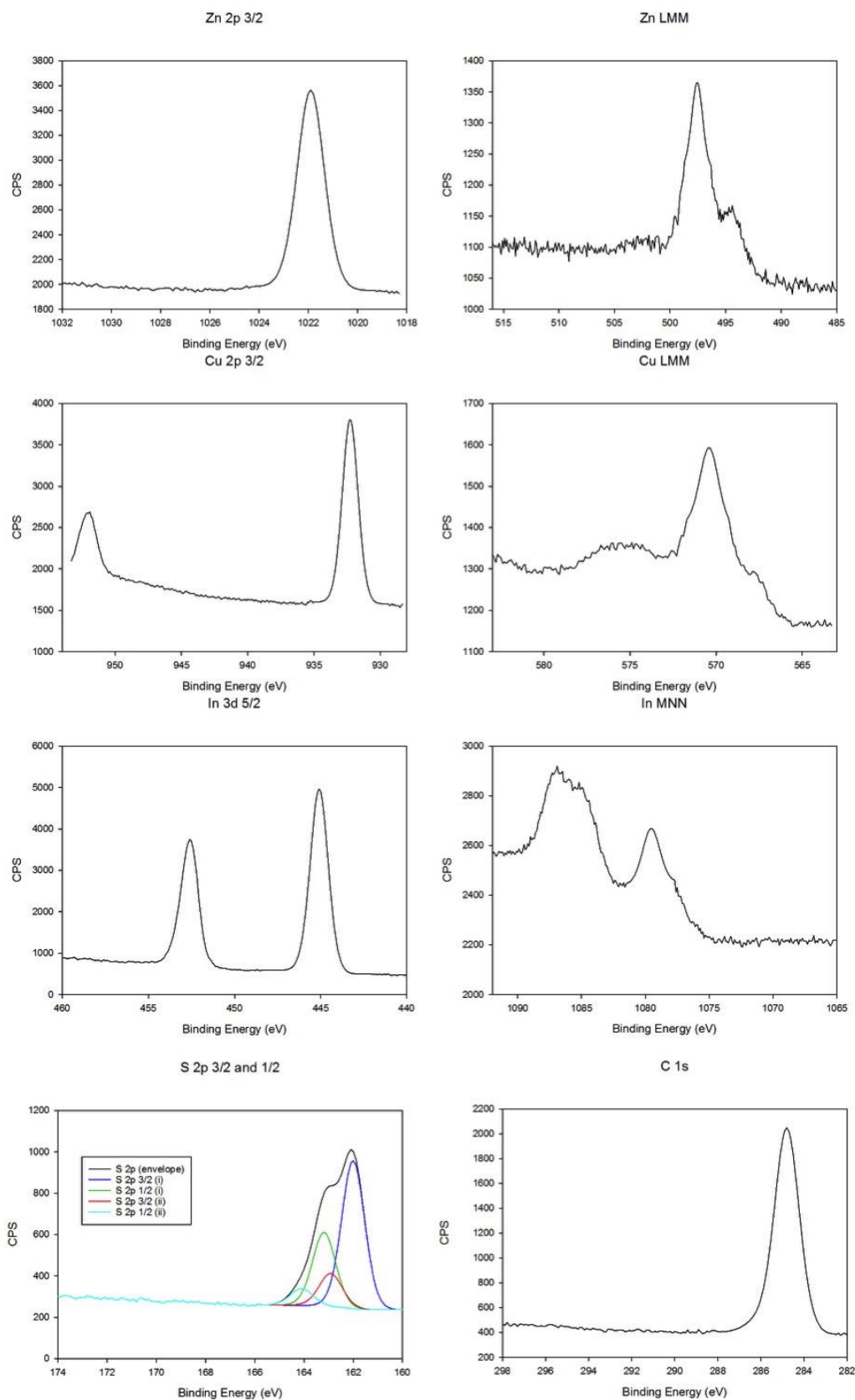
Figure 3-4: High Resolution XPS Scans for ZCIS R1 Peaks.

Table 3-4: XPS Peak Positions

Peak	Peak Position (eV) (ZCIS R1)		Dominant Species/Compound (Beamson 1992, Wagner 2003, Biesinger, 2010)
Zn 2p 3/2	1021.90		
Zn LMM	497.55 Auger Parameter: 2011.1		**Zn(II) – Zn$_2$S**
Cu 2p 3/2	932.27		**Cu(I) - CuS**
Cu LMM	570.40 Auger Parameter: 1848.6		**Cu(I) - CuS**
In 3d 5/2	445.08		**CuInS$_2$**
In MNN	1079.55 Auger Parameter: 852.2		**In$_2$S$_3$**
S 2p 3/2	162.01(i) (82%)	162.92(ii) (18%)	**CuS, C-S-H (Thiol), (CuInS$_2$)**
S 2p 1/2	163.19(i)	164.10(ii)	**Doublet separation from S 2p 3/2, +1.18 eV**
C 1s	284.80		**C-C, C-H (from QD ligand)**

Comparing the binding energies for each peak to those in XPS databases (Beamson 1992, Wagner 2003), confirms the chemical structure of the QD sample as being a mix of Zn$_2$S, CuS, In$_2$S$_3$, CuInS$_2$, and C-C / C-H bonds from the QD ligand. Analyzing the auger parameters as well for zinc, copper, and indium allows for more insight into the dominant chemical species, as there is limited availability of XPS database data for specific binding energies from CuInS$_2$. The zinc peaks indicate Zn(II) as being the dominant species. The copper peaks indicate Cu(I) as being the dominant species. The indium auger parameter suggests In$_2$S$_3$ as being the dominant species, however the indium 3d 5/2 peaks correspond directly to the binding energy of CuInS$_2$, 444.9 +/- 0.4 eV (Wagner 2003). This suggests that there is a mixture of metal sulfides present in the sample, a commonly found result in literature (Lee, 2014). The C 1s peaks shows C-C

and C-H as being the dominant species, which was expected from the ligand functionalization on the QDs.

X-ray Diffraction:

ZCIS QD samples from each reaction resulted in a similar crystal structure with varying degrees of intensity, caused by different QD sizes. The dominant structure was found to be tetragonal chalcopyrite CIS, with characteristic peaks at 27, 47 and 55 degrees. Peaks emerging at 68 and 75 degrees correspond to ZnS(Chang and Waclawik 2013). The differences in peak intensity arise from slightly different particle sizes, with smaller peaks indicating smaller QD size. The peak locations from each sample occur at the same position, indicating the same crystal structure is present in each QD sample.
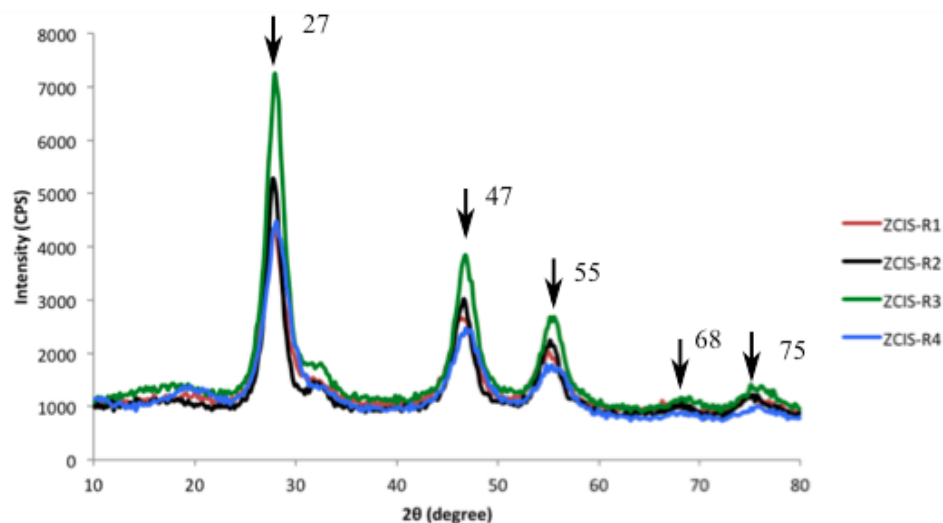
Figure 3-5: XRD results for ZCIS QDs with 60 minute reaction time.

Photoluminescence Spectroscopy:

Photoluminescent emission profiles of the zinc copper indium sulfide (ZCIS) QDs collected ranged from 575-725 nm, as shown in Figure 3-6. The ZCIS samples all had much lower emission intensities than the CIS QDs, with none exceeding 10 000 counts.
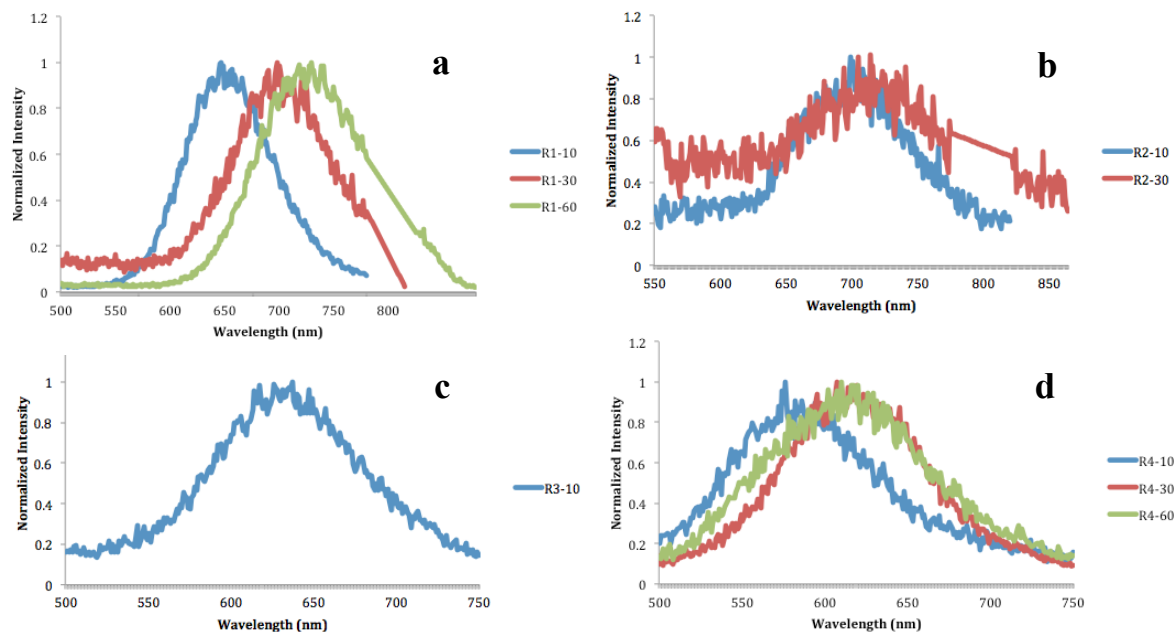
Figure 3-6: Emission Spectrum of ZCIS QDS with different molar ratios, Zn:Cu:In, and different reaction times, labeled in minutes. ZCIS-R1 (a), ZCIS-R2 (b), ZCIS-R3 (c), and ZCIS-R4 (d).

The clear effect of reaction time on the photoluminescent emission spectrum can be seen in Figure 3-6. Longer reaction time allows for more crystal growth and a red shifted emission spectrum. For reactions R2 and R3, labeled b and c, the emission spectrum reached equilibrium after 10 minutes of reaction time, with samples collected after 10 minutes showing very low photoluminescent emission. Reaction R4, d, used the same molar ratio of Cu:In, 1:2, which was found to be optimal in the original QD reactions without zinc. Based on the emission spectrums from 30 and 60 minutes of reaction time, the majority of QD growth was complete after 30 minutes (d). The spectrums for 30 and 60 minutes have the same emission peak at approximately 620 nm, however the spectrum from the 60 minute sample has a wider distribution, potentially indicating a larger distribution of QD size (d). Furthermore EDX results indicated a very similar elemental composition between samples taken at 10 and 60 minutes of reaction time. Additional reaction time leads to widening of the emission spectrum caused by an increase in the range of particle sizes. Sample QDs dispersed in toluene under 365 nm UV lamp illumination can be seen below in Figure 3-7.
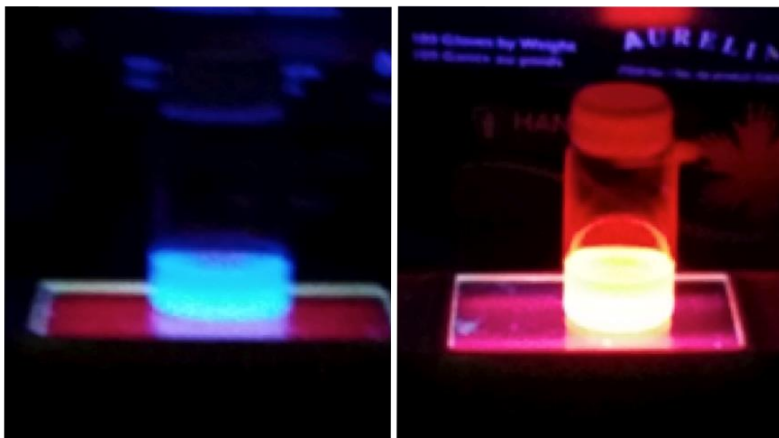
Figure 3-7: ZCIS QDs dispersed in toluene under 365 nm illumination (left) and CIS QDs dispersed in toluene under 365 nm illumination (right).

Nanocomposite Thin-Film Samples:

QDs-EVA nanofilms were prepared by incorporating CIS QDs into EVA films. ZnO-EVA films were also prepared using commercial nano-ZnO for comparison. The effect of loading percentages of zinc oxide and CIS QDs on the transmittance can be seen below in Figures 3-8 and 3-9, respectively. Increasing loading causes a reduction in UV transmittance, meaning more of the light is being absorbed by the QD-EVA films. However there is a slight tradeoff when increasing UV absorbance. Transmittance in the visible region is also decreased, which will reduce the overall efficiency of the application. Using a lower loading percentage and thinner films equates to less QDs required and a lower overall cost. Finding a balance between low QD loading and high UV absorbance is essential.

UV-Visible Spectroscopy:
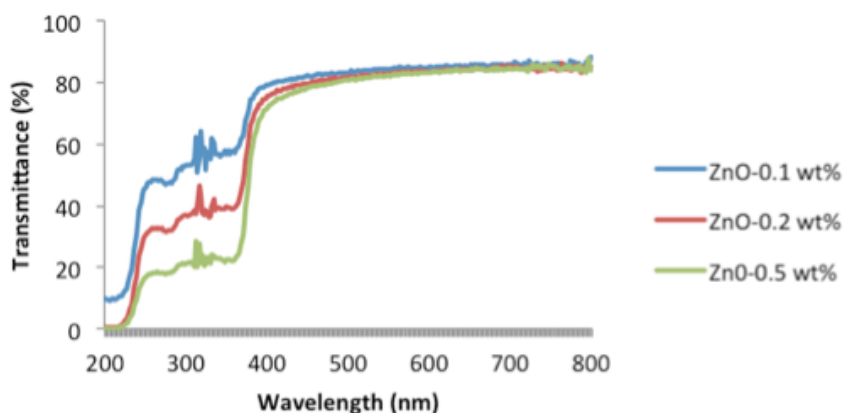
Figure 3-8: Transmittance Spectrum of 250 μm Zinc Oxide-EVA Thin Films.

ZnO-EVA thin films show reduced transmittance throughout the UV region, especially between 250-350 nm. The wt.% ZnO is directly proportional to the amount of light being absorbed by the thin film.
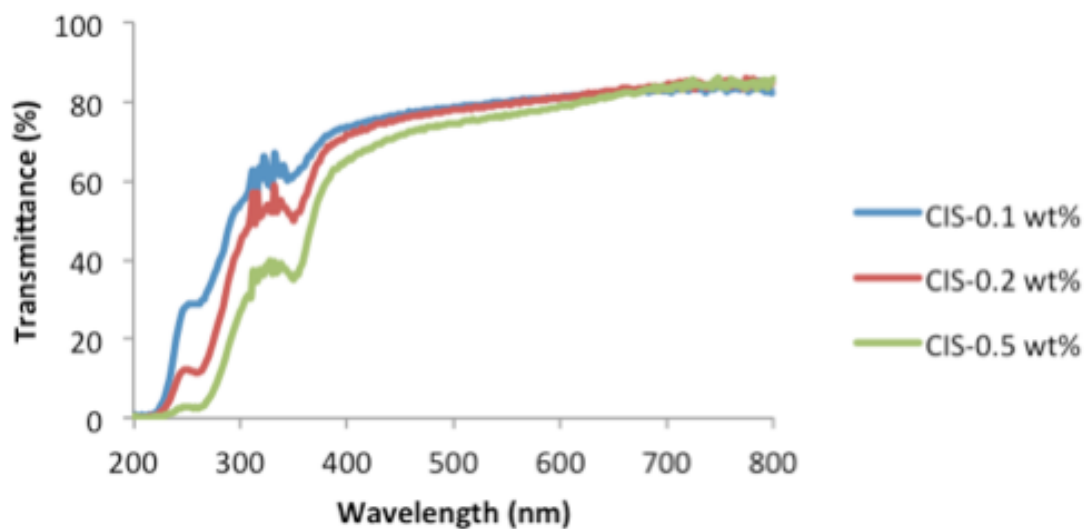
Figure 3-9: Transmittance Spectrum of 250 μm CIS-R1-HU-EVA Thin Films.

CIS-EVA thin films show a reduced transmittance throughout the UV region (200-400nm) that is directly proportional to CIS QD wt.%.

Table 3-5: Summary of ZnO - EVA and CIS-R1-HU - EVA Thin Films

Sample	Average UV Transmittance (%)
ZnO – 0.1 wt% 250 μm	48.0
ZnO – 0.2 wt% 250 μm	34.0
ZnO – 0.5 wt% 250 μm	22.3
CIS – 0.1 wt% 100 μm	60.0
CIS – 0.1 wt% 250 μm	43.6
CIS – 0.2 wt% 250 μm	35.2
CIS – 0.5 wt% 250 μm	24.7

From Table 3-6 it can be seen that both film materials prepared using CIS and ZnO have similar transmittance values for equal weight percentages. As expected, increasing the loading percentage or film thickness caused a decrease in UV transmittance because more QDs were present to absorb the light. It is also clear that when doubling the loading percentage, the amount of light being absorbed by the material only increases by about 20-30 %.

When comparing average UV transmittance from the different CIS QD samples (Table 3-5 and 3-6), CIS-R1-HI and CIS-R1-HU, it can be observed that the CIS-R1-HU films allow less UV transmission. This is attributed to QDs in these films having higher QY and stronger absorbance, as confirmed from the Chapter 2 results.

Table 3-6: Summary of CIS-R1-HI - EVA Thin Films

Sample	Average UV Transmittance (%)
CIS –0.1 wt% 100 μm	67.1
CIS – 0.1 wt% 250 μm	55.5
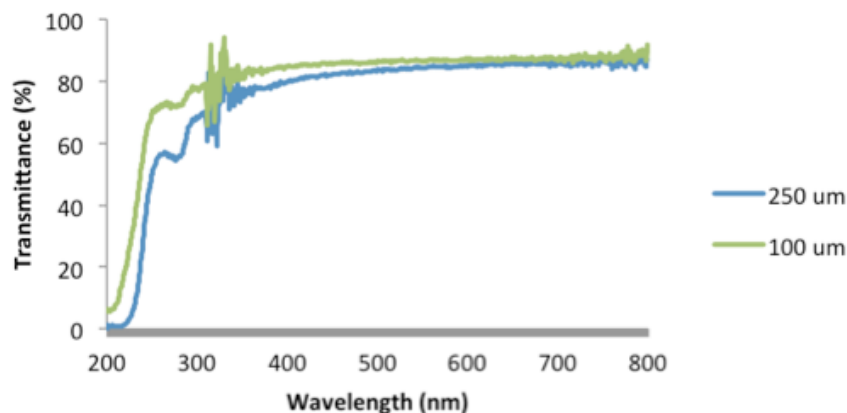
Figure 3-10: Transmittance Spectrum of 0.1 wt.% CIS-R1-HI-EVA Thin Films.

One of the main issues with QDs is their degradation caused by oxidation. This makes effectively storing and using them more difficult. Commercial QDs remain stable from oxidation for approximately 6-24 months if kept in optimal storage conditions, low temperature and sealed from light exposure(Crystalplex 2014, Mesolight 2014). It is essential to make the QDs more stable for light conversion applications. To see the effects of aging in ambient conditions on the CIS-EVA films, absorbance profiles collected immediately after film assembly were compared to those collected after 11 months of aging in ambient conditions, Figure 3-11.
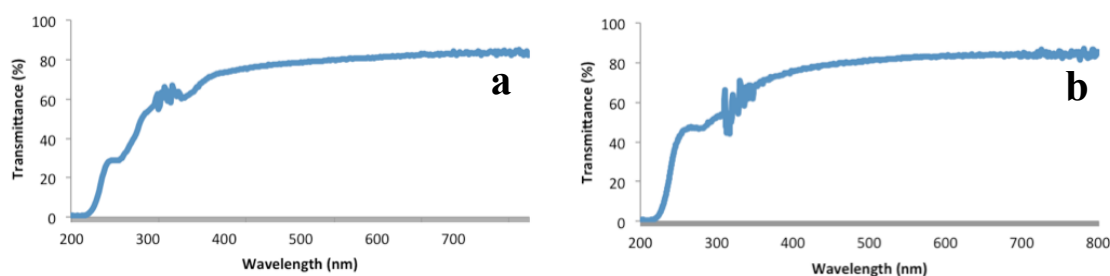
Figure 3-11: Transmittance Spectrum of 250 μm, 0.1 wt.% CIS-EVA thin film after fabrication (a) and aged 11 months (b).

Table 3-7: Summary of CIS-R1-HU - EVA Thin Films Aged 11 Months

Sample	Average UV Transmittance (%)
Initial	43.6

Aged	47.7
Transmittance Increase	4.1

These results indicate excellent stability of the QDs in the polymer matrix. The films remain transparent and show no visual signs of photo bleaching, a photochemical change in the QDs making them less fluorescent, caused by reactions between the QDs and surrounding molecules. This indicates that the ligand, 1-dodecanethiol, used to functionalize the QDs is highly compatible with the selected polymer, EVA 1075.

Scanning Electron Microscopy:

Images were taken of 250 μm films at different magnifications, 100x, 1000x, and 10 000x to compare the effect of different of different QD loading percentages.
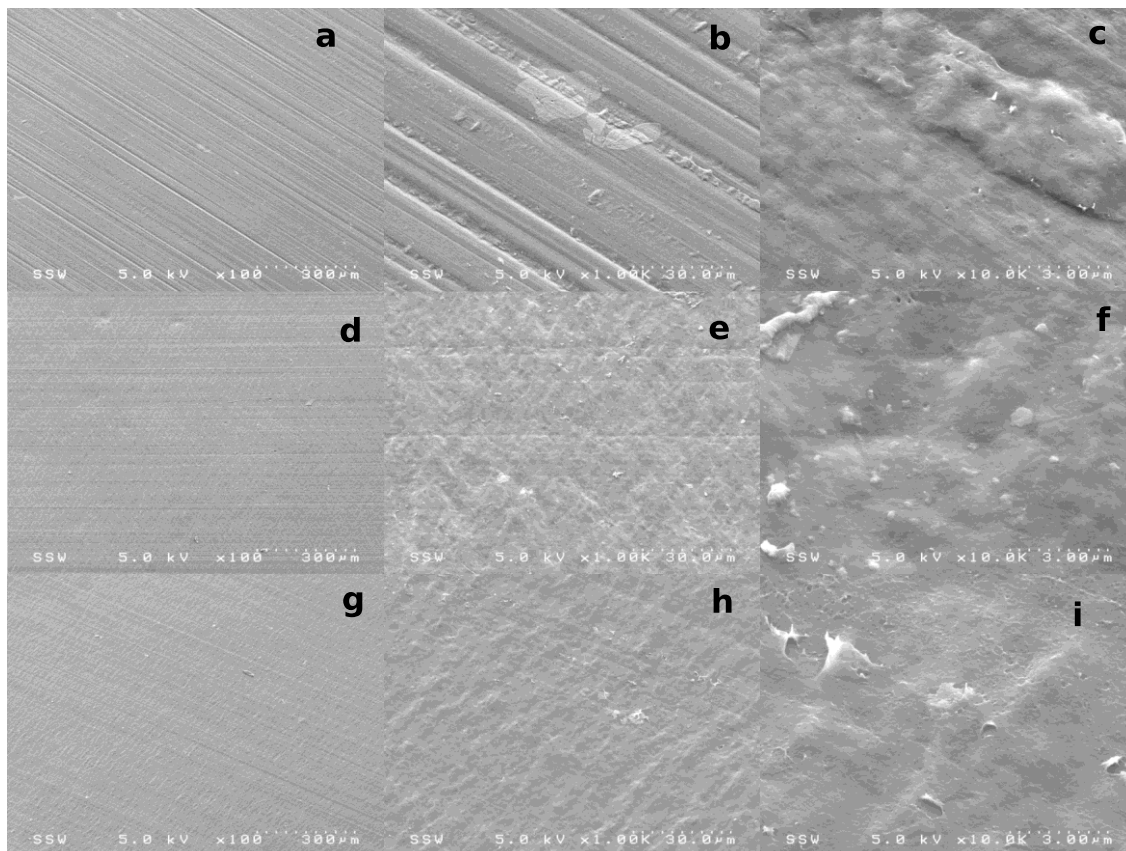
Figure 3-12: SEM image 0.1 wt% CIS QD in EVA at 100x mag (a), 1000x mag (b), and 10 000x mag (c). 0.2 wt% CIS QD in EVA at 100x mag (d), 1000x mag (e), and 10 000x mag (f). 0.5 wt% CIS QD in EVA at 100x mag (g), 1000x mag (h), and 10 000x mag (i).

As expected, when comparing the different loading percentages, it was found that an increased QD loading percentage resulted in more distortions on the film surface. This can be seen best by comparing Figure 3-12 images c, f, and i.

Potential Efficiency Increases for Silicon Solar Cells

Due to the relatively low QY of QDs used in this work, resulting QD-EVA thin films applied to actual solar cells would provide a negligible increase in efficiency. However commercially available CIS QDs have QYs as high as 70-80%, making them capable of providing substantial increases in efficiency(Nanoco-Group-PLC 2014). The table below summarizes potential efficiency increases from using commercial QDs for down-conversion. The calculations assume that all UV light not transmitted through the film is effectively absorbed by the QDs. Although some light would obviously be

diffused through the film and not absorbed fully, it can be assumed that the UV absorbance of commercial QDs is much higher than that of those used to collect UV transmission data in this work. A total solar irradiance of 1000 W/m^2 was assumed with 149 W/m^2 of light available for down-conversion and 468 W/m^2 currently being absorbed by a 15% efficient silicon cell(Yao Zhu 2013). Efficiency increases are provided based on QYs of 30 and 80 %.

Table 3-9: Potential efficiency increases from a down-conversion layer for silicon solar cells

Sample Name	UV Light Absorbed (%)	Predicted Efficiency Increase (%)	
CIS 0.1wt% 100 μm	40	30% QY	80% QY
		0.6	**1.5**
CIS 0.1wt% 250 μm	56	30% QY	80% QY
		0.8	**2.1**
CIS 0.2wt% 250 μm	65	30% QY	80% QY
		0.9	**2.5**
CIS 0.5wt% 250 μm	75	30% QY	80% QY
		1.1	**2.9**
ZnO 0.1wt% 250 μm	52	30% QY	80% QY
		0.7	**2.0**
ZnO 0.2wt% 250 μm	66	30% QY	80% QY
		0.9	**2.5**
ZnO 0.5wt% 250 μm	78	30% QY	80% QY
		1.1	**3.0**

Due to the low loading percentages and thin films, only a small amount of QD material is required for this application. Assuming the density of EVA 1075 is 0.924 g /cm^3(Holland 2015), a 100 μm thin film would require 0.92-4.6 g of QDs per m^2 and a 250 μm thin film would require 2.3- 11 g of QDs per m^2.

Conclusion:

This work investigated the use of CIS QDs in down converting nanocomposite thin films and their potential for allowing zinc with CIS QDs to modify their emission spectrum. Alloying with different molar ratios of zinc allowed the emission spectrum to be shifted from 575-725 nm. The effect of different film thickness, QD material, and

loading percentage was examined. It was found that film thickness and loading percentage were directly related to UV transmission. Previous studies on QD-EVA thin films using cadmium sulfide QDs reduced average UV transmission to as low as 75% with a cadmium sulfide wt% loading of 0.5% and 250 μm film thickness (Allan et al. 2014). QD-EVA thin films from this work reduced average UV transmission down to 25%, a substantial improvement. Films were found to have good long term stability and show potential for utilizing higher quality, commercial QDs to provide efficiency increases up to 3% for first generation silicon based solar cells.

Bibliography

1.   Allan, J.M. (2012). Light and Heat Selective Polymer Nanocomposite Films for Sustainable Greenhouses. M.E.Sc., The Univerisity of Western Ontario.
2.   Allan J.M., Mumin M.A., Xu W.X., AlSharari Q.,Charpentier P.A. (2014) "Surface functionalized bare and core–shell quantum dots in poly (ethylene-co-vinyl acetate) for light selective nanocomposite films." Solar Energy Materials and Solar Cells. Volume 123: 30–40.
3.   Baker, A. L. e. a. (2012). "Phycokey -- an image based key to Algae (PS Protista), Cyanobacteria, and other aquatic objects." 2015, from http://cfb.unh.edu/phycokey/phycokey.htm
4.   Beamson, G. and Briggs, D. High Resolution XPS of Organic Polymers - The Scienta ESCA300 Database Wiley Interscience, 1992.
5.   Biesinger, M.C., Lau, L.W.M., Gerson, A.R., Smart, R.St.C. Appl. Surf. Sci. 257 (2010) 887.
6.   Chang, J. and E. R. Waclawik (2013). "Controlled synthesis of CuInS2, Cu2SnS3 and Cu2ZnSnS4 nano-structures: insight into the universal phase-selectivity mechanism." CrystEngComm 15(28): 5612.
7.   Choi, S. H., E. G. Kim and T. Hyeon (2006). "One-pot synthesis of copper-indium sulfide nanocrystalheterostructures with acorn, bottle, and larva shapes." J Am ChemSoc 128(8): 2520-2521.
8.   Guijarro, N., E. Guillen, T. Lana-Villarreal and R. Gomez (2014). "Quantum dot-sensitized solar cells based on directly adsorbed zinc copper indium sulfide colloids." PhysChemChemPhys 16(19): 9115-9122.
9.   Han, W., L. Yi, N. Zhao, A. Tang, M. Gao and Z. Tang (2008). "Synthesis and shape-tailoring of copper sulfide/indium sulfide-based nanocrystals." J Am ChemSoc 130(39): 13152-13161.
10.   Holland, M. (2015). "Ateva® 1075A - Celanese EVA Performance Polymers - Ethylene Vinyl Acetate Copolymer." from http://catalog.ides.com/Datasheet.aspx?I=18647&E=75386.

11. Katsuhiro Nose, T. O., and Shinya Otsuka-Yao-Matsuo (2008). "Colloidal Synthesis of Ternary Copper Indium Diselenide Quantum Dots and Their Optical Properties." Journal of Physical Chemistry 113: 3455-3460.
12. Lee, J., & Han, C.-S. (2014). Large-scale synthesis of highly emissive and photostable CuInS2/ZnS nanocrystals through hybrid flow reactor. Nanoscale Research Letters, 9(1), 78. 1556
13. Mesolight. (2014). "Quantum Dot Products." from http://www.mesolight.com/index.php.
14. Nanoco-Group-PLC. (2014). "Quantum Dots manufactured in Bulk Quantities." 2014, from http://www.nanocotechnologies.com/index.aspx.
15. Nanotech, O. (2014). "Products Catalogue ", from http://www.oceannanotech.com/catalog.php.
16. NREL. (2012). "Novel Physical Principles Research Thrust." 2015, from http://www.centerforadvancedsolarphotophysics.org/physical_principles.html.
17. NREL. (2014). "National Center for Photovoltaics." 2015, from http://www.nrel.gov/ncpv/.
18. Queisser, W. S. a. H. J. (1961). "Detailed Balance Limit of Efficiency of p- n Junction Solar Cells." Journal of Applied Physics 32: 510-519.
19. SISER. (2014). "Up and Down-conversion." from http://siser.eps.hw.ac.uk/research/next-generation/up-and-down-conversion.
20. Song, W.-S. and H. Yang (2012). "Efficient White-Light-Emitting Diodes Fabricated from Highly Fluorescent Copper Indium Sulfide Core/Shell Quantum Dots." Chemistry of Materials 24(10): 1961-1967.
21. Svrcek V, S. A., and Muller JC (2004). "Silicon nanocrystals as light converter for solar cells." Thin Solid Films 451: 384-388.
22. Wagner C.D., Naumkin A.V., Kraut-Vass A., Allison J.W., Powell C.J., Rumble J. NIST Standard Reference Database 20, Version 3.4 (web version) (http:/srdata.nist.gov/xps/) 2003.
23. W.G.J.H.M. van Sark, A. M. a. R. E. I. S. (2012). Solar Spectrum Conversion for Photovoltaics Using Nanoparticles. Third Generation Photovoltaics. D. V. Fthenakis, INTECH.
24. Xu W.Z., and Charpentier P.A. (2009). "Light-Selective Nanofilms of Quantum Dot-Poly(ethylene-co-vinyl acetate) Synthesized with Supercritical CO2." The Journal of Physical Chemistry C2009113 (16), 6859-6870.
25. Yao Zhu, A. A., Bruno Masenelli and Patrice Melinon (2013). "Zinc oxide nanoparticles as luminescent down-shifting layer for solar cells." SPIE.
26. Yu, K., P. Ng, J. Ouyang, M. B. Zaman, A. Abulrob, T. N. Baral, D. Fatehi, Z. J. Jakubek, D. Kingston, X. Wu, X. Liu, C. Hebert, D. M. Leek and D. M. Whitfield (2013). "Low-temperature approach to highly emissive copper indium sulfide colloidal nanocrystals and their bioimaging applications." ACS Appl Mater Interfaces 5(8): 2870-2880.

CONCLUSION:

This work investigated the synthesis and application of CIS QDs. Samples produced from three different synthesis methods, two based on hydrothermal approaches and one microfluidic synthesis, were compared based on their optical and structural properties. It was found that the HU and microfluidic techniques produced QDs with higher QYs. This was expected for the microfluidic approach, however the difference in samples produced from the two hydrothermal syntheses was an interesting discovery. Previous reports suggest that by introducing the ligand into the reaction solution prior to initiating the reaction a more stable product will be formed. Although the size distribution of samples for the HI synthesis is smaller, it still results in a lower QY compared to the HU synthesis. This is an intriguing result because most reports in literature imply that QDs with a more narrow size distribution are of higher quality. However this also depends on the QD's end application.

QD-EVA nanocomposite thin films produced in this work are an excellent proof of concept for using CIS QDs in a down-conversion layer to improve efficiency in first generation solar cells. To the best of my knowledge using CIS QDs for this concept has not previously been reported. By utilizing higher quality CIS QDs, such as those from a commercial source, efficiency gains for a first generation solar cell could be as high as 2-3 %. The high degree of tunability for the emission spectrum of CIS QDs, by alloying with zinc, would allow them to be applied to any solar cell utilizing silicon with a band gap in the range of 550-950 nm. Furthermore, this technology would provide an excellent stepping-stone for manufacturers of first generation photovoltaics. It can be easily integrated into the current manufacturing process simply by pre-treating the EVA before it is applied as the final lamination layer on the solar cell. Although third generation solar cells are capable of reaching much higher efficiencies their manufacturing process requires very expensive processing techniques, making them unattractive to current commercial photovoltaic manufacturers.

FUTURE WORK:

Results from this work indicate excellent potential for continued research on the use of CIS QDs as a down-conversion material. By utilizing commercial CIS QDs from manufactures like Mesolight, Nanoco, or Crystalplex, resulting QD-EVA thin films would be very promising for enhancement of first generation solar cells. However, developing the QD-EVA thin films into commercially viable technology will require optimization of large-scale production of QDs, due to the high cost of all currently available commercial QDs. For continued research on the greenhouse application of QD-EVA thin films, a strategy involving a combination of ZnO and CIS QDs in EVA would be promising. These films could be capable of emitting light from 400-520 nm and from 650-675 nm, matching the optimal wavelengths of light required to drive photosynthesis in plants. Different QD surface ligands could be experimented with to compare their compatibility with EVA, although 1-dodecanthiol showed minimal signs of degradation after 11 months of aging. Processing with supercritical CO_2 to embed the CIS QDs in the polymer would also be a beneficial study to produce QD-EVA thin films form an alternative technique.

Continued research on the development of a microfluidic synthesis system for producing QDs will ensure high quality, reproducible products. Developing more expertise and experimenting with different fabrication procedures will improve the current results using CIS QDs as the primary absorbing layer in QDSSCs.

APPENDIX:

Microfludic Reactor Setup:

XPS Database Figures:

Substance	BE (eV)	St. Dev. (eV)	# of Ref.
C-S-C (Sulphide, Sulfide)	163.7	0.6	15
C-S-H (Thiol)	163.8	0.4	7
C4S-H (Thiophene)	164.0	0.3	11
R2-SO (Sulphinyl, Sulfinyl)	165.5	0.5	5
C-SO2-C (Sulphone, Sulfone)	167.7	0.3	5
C-SO3-H, C-SO3-Na (Sulphonate, Sulfonate)	168.1	0.2	3

(Beamson 1992, Wagner 2003)

Species	Cu 2p3/2 B.E. (eV)	St. Dev. (eV)	# of Ref.	Cu 2p3/2 Cu LMM Auger Parameter	St. Dev. (eV)	# of Ref.	S 2p3/2 B.E. (eV)	St. Dev. (eV)	# of Ref.
Cu2S	932.5	0.2	9	1849.8	0.2	3	161.9	0.4	9
CuS	932.2	0.2	7	1850.3	0.2	3	162.1	0.6	5

(Beamson 1992)

Compound	Binding Energy (eV)	Std. Dev.	# of Lit. Ref.
CuS (Covellite)	162.1	0.6	16
CuS2 (Chalcocite)	161.9	0.4	13
FeS (Pyrrhotite/Trolite)	161.1	0.4	2
FeS2 (Pyrite)	162.5	0.5	4
CuFeS2 (Chalcopyrite)	161.5	0.1	2
NiS (Millerite)	162.1	0.7	5
Ni3S2 (Heazlewoodite)	163.0		1
ZnS (Sphalerite)	161.6	0.3	7
PbS (Galena)	160.6	0.6	4
PtS (Cooperite)	163.4	0.4	2
WS2	162.6	0.4	7
SnS	161.1		1
AgS2 (Acanthite)	160.8	0.1	2
Co9S8	162.9	0.2	2

(Beamson 1992)

In 3d 5/2

Species	B.E. (eV)	Std. Dev. (eV)	# of Ref.
In(0)	443.8	0.3	42
In(OH)3	445.1	0.1	2
In2O3	444.8	0.6	15
CuInSe2	444.6	0.3	4
In2S3	445.1	0.4	4
In2Se3	444.8	0.3	3
In2Te3	444.5	0.1	2
InBr3	446.1	0.5	3
InCl3	446.3	0.6	3
InF3	446.4	0.2	2
InI3	445.6	0.6	3
InP	444.6	0.5	9
InSb	444.5	0.1	2
CuInS2	444.9	0.4	4

(Beamson 1992)

Compound	Zn 2p3/2 (eV)	Std. Dev. (+/- eV)	Zn 2p1/2 (eV)	Std. Dev. (+/- eV)	Zn 2p1/2 - Zn 2p3/2 Splitting (eV)	FWHM (eV), 10 eV Pass Energy, Zn 2p3/2	FWHM (eV), 10 eV Pass Energy, Zn 2p1/2	FWHM (eV), 20 eV Pass Energy, Zn 2p3/2	FWHM (eV), 20 eV Pass Energy, Zn 2p1/2	Modified Auger Parameter (eV)	Zn 2p3/2 (eV) (Lit. Ave)	Std. Dev. (+/- eV)	# of Citations	Modified Auger Parameter (eV) (Lit. Ave.)	Std. Dev. (+/- eV)	# of Citations
Zn(0) (a)	1021.65	0.01	1044.66	0.01	23.01	0.82	1.00	0.86	1.04	2013.77	1021.62	0.38	15	2013.85	0.25	13
Zn(II) Oxide	1021.00	0.04	1044.11	0.04	23.11	1.55	1.59	1.60	1.63	2010.40	1021.96	0.53	16	2010.14	0.39	9

a) Assymetric peakshape LA(1.4,2,2)

[1] M.C. Biesinger, L.W.M. Lau, A.R. Gerson, R.St.C. Smart, Appl. Surf. Sci. 257 (2010) 887

Standard dyes based on useful excitation range (Nanoco-Group-PLC 2013)

Standard	Supplier	Solvent	QY	Fluorescence max (nm)	Useful excitation range (nm)
9, 10-diphenylanthracene	Acros	Ethanol	0.90	406, 427	320-370
Coumarin 1	Aldrich	Ethanol	0.73	450	320-370
Coumarin 153	**Aldrich**	**Ethanol**	**0.58**	**530**	**370-450**
Rhodamine 123	Aldrich	Ethanol	0.95	535	440-490
Rhodamine 6G	Aldrich	Ethanol	0.95	560	450-500
Sulphohodamine 101	Aldrich	Ethanol	0.90	600	500-550

CURRICULUM VITAE

Harrison Ward

EDUCATION

Master of Engineering Science, M.E.Sc. Chemical Engineering **Sept 2013-Present**
The University of Western Ontario, London, ON
- Research focus: new materials for improving solar cell efficiency
- Thesis title: "Copper Indium Sulfide Quantum Dots for Light Selective Nanocomposite Films and Solar Cell Applications"

Bachelor of Engineering Science, B.E.Sc. Green Process Engineering **Sept 2009-Apr 2013**
The University of Western Ontario, London, ON
- Program Focus: Environmental, Chemical, and Renewable Energy Systems Engineering

ENGINEERING WORK EXPERIENCE

Graduate Research Assistant **Sept 2013-Present**
The University of Western Ontario, Charpentier Research Group, London, ON
- Complete project reviews for the Research Group's industry partners, Enerworks Inc. and MW Canada
- Prepare and analyze samples for fellow graduate students using Transmission Electron Microscopy
- Assist fellow graduate students with Photoluminescence Spectroscopy, UV-Visible Spectroscopy, and experimental design
- Proficiency with variety of chemical synthesis techniques

Mitacs-s2e Technologies Inc. Intern **Sept-Dec 2013**
Mitacs-s2e Technologies Inc., London, ON
- Modeled potential solar cell efficiency increases based on early research results from my master's thesis
- Presented research results from master's thesis in technical reports and presentations to industry leaders and professors
- $15 000 scholarship for collaborative research project connecting students to companies in industry
- Coordinated work efforts with several different research teams to complete a final report

Summer Research Student **May-Aug 2013**
The University of Western Ontario, London, ON
- Assessed experiments completed by fellow research group members and prepared technical reports based on the findings
- Learned operating procedures for complex material analysis techniques and became self proficient

ACADEMIC PROJECTS

Green Process Laboratory Research Project   **Sept 2012-Apr 2013**

The University of Western Ontario, London, ON

- Reduced the toxicity of a solar cell material previously used in my supervisor's laboratory, without degrading performance
- Collaborated with fellow research group members on experimental design, analytical techniques, and report preparation

Green Process Design   **Sept 2012-Mar 2013**

The University of Western Ontario, London, ON

- Designed bitumen upgrading facility, including process modeling, equipment selection, and GHG assessment
- Awarded by the Faculty of Engineering for showing excellence in engineering design

Blue Forest Environmental Development Project   **Sept 2012-Dec 2012**

The University of Western Ontario, London, ON

- Awarded $1 200 from industry company for developing a geographic pricing model for waste disposal alternatives in Southwestern Ontario
- Presented findings in a technical report and won an industry judged presentation

AWARDS AND ACHIEVEMENTS

The University of Western Ontario Gold Medal in Green Process Engineering   **June 2013**

The University of Western Ontario, London ON

- Highest marks in the Green Process Engineering program

Dr. James A Vance Prize   **June 2013**

The University of Western Ontario, London ON

- Excellence in engineering design as determined by the Faculty of Engineering

CERTIFICATIONS

Laboratory Safety – Hazardous Waste   **July 2013**

The University of Western Ontario, London, ON

Comprehensive Workplace Hazardous Materials Information System Training   **June 2013**

The University of Western Ontario, London, ON

Western Green Campus Program   **Sept 2012-Feb 2013**

The University of Western Ontario, London, ON

- Completed four workshops relating to sustainability, LEED certifications, waste management, and biodiversity

CLUBS

Chem-E-Car   **Sept 2011-Mar 2012**

The University of Western Ontario, Chem Club, London, ON
- Performed lab tests to optimize car design and methanol fuel requirements for contest challenges